Monthly Notices of the ROYAL ASTRONOMICAL SOCIETY

MNRAS **535,** 2449–2468 (2024) https://doi.org/10.1093/mnras/stae2453
Advance Access publication 2024 October 29

The Meissner effect in neutron stars

S. K. Lander★
School of Engineering, Mathematics and Physics, University of East Anglia, Norwich NR4 7TJ, UK

Accepted 2024 October 24. Received 2024 October 24; in original form 2024 September 2

ABSTRACT

We present the first model aimed at understanding how the Meissner effect in a young neutron star affects its macroscopic magnetic field. In this model, field expulsion occurs on a dynamical time-scale, and is realized through two processes that occur at the onset of superconductivity: fluid motions causing the dragging of field lines, followed by magnetic reconnection. Focusing on magnetic fields weaker than the superconducting critical field, we show that complete Meissner expulsion is but one of four possible generic scenarios for the magnetic-field geometry, and can never expel magnetic flux from the centre of the star. Reconnection causes the release of up to $\sim 5 \times 10^{46}$ erg of energy at the onset of superconductivity, and is only possible for certain favourable early-phase dynamics and for pre-condensation fields $10^{12}\,\mathrm{G} \lesssim B \lesssim 5 \times 10^{14}\,\mathrm{G}$. Fields weaker or stronger than this are predicted to thread the whole star.

Key words: stars: magnetic fields – stars: neutron.

1 INTRODUCTION

The hallmark of superconductivity in a material is the Meissner(-Ochsenfeld) effect, characterized by an expulsion of magnetic flux and occurring once the temperature T drops below some critical value T_c. The nature of the expulsion depends on the strength B of the magnetic field through the material prior to the onset of superconductivity. For weak fields, there is a complete expulsion of flux from the interior of the superconducting sample; for sufficiently strong fields, superconductivity is destroyed and the conductivity is normal; for intermediate field strengths, there is a partial expulsion of flux. The nature of this latter state depends on the kind of superconductivity that is operative, but generally is characterized by narrow structures of concentrated flux that have returned to the normal regime, surrounded by superconducting regions with zero magnetic field.

In the laboratory, the magnetic field is imposed on a sample externally, and once cooled below T_c the sample sets up a supercurrent that screens the external field and ensures the sample harbours no internal magnetic flux. But this effect is also important in astrophysics, being operative in one class of magnetic stars: neutron stars (NSs). The extremely high density of an NS core leads to a correspondingly high critical temperature for superconductivity, and efficient neutrino cooling allows the star to drop below this value shortly after birth.

A few features of the physics of NSs indicate that any magnetic-flux rearrangement occurring due to the transition to superconductivity will differ from the Meissner effect familiar from terrestrial physics. For one, their magnetic field is internal to the star, produced by the persistent electric currents within the stellar fluid. As the Meissner effect is not intrinsically dissipative, it is less obvious how to expel this field than in the laboratory setup. Secondly, T_c varies considerably throughout the core and is highest close to the crust–core boundary; the Meissner effect will therefore proceed gradually, on the cooling time-scale, and rather than expelling the core magnetic field may instead trap some of it. Finally, terrestrial superconductors are solid, and the electron fluid becomes superconducting. An NS core is entirely fluid, and instead of the low-mass electrons, it is the proton fluid which forms a superconductor. Because the neutrons, with their lower critical temperature, only become superfluid considerably later on, the core may be treated as a single fluid at the onset of superconductivity. We are therefore in a magnetohydrodynamic (MHD) regime, with the additional restrictions that places on the fluid flow, and therefore on how Meissner expulsion may be realized.

The aim of this paper is to explore how the Meissner effect operates in this setting, and what the result is likely to be on the star's large-scale magnetic field.

2 THE ONSET OF SUPERCONDUCTIVITY: TERRESTRIAL VERSUS NEUTRON-STAR CONDITIONS

Superconductivity occurs when it becomes energetically favourable for two fermions to become coupled into a Cooper pair, notwithstanding the Coulomb repulsion between them. In terrestrial materials, it is the electrons in the medium that may form Cooper pairs; in NS cores, the proton fluid. The critical temperature, below which pairing sets in, depends upon the properties of the medium, and is well understood for low-temperature superconductors – generally defined, in the terrestrial case, as those for which $T_c < 77\,\mathrm{K}$, the boiling point of liquid nitrogen. For NS cores, the typical value is rather higher than this, $T_c \sim 10^9\,\mathrm{K}$, due to their vastly higher densities. This means that it is still appropriate to treat them with the standard theory of low-temperature superconductivity, whose fundamentals are covered in several textbooks (we frequently draw upon Tinkham 2004 here). For temperatures $T > T_c$, superconductivity is destroyed, and the medium behaves according to the usual equations of classical

★ E-mail: samuel.lander@uea.ac.uk

electrodynamics. Analogous to T_c, there also exists a critical field strength H_c: superconductivity can be destroyed by increasing the magnetic-field strength B beyond H_c, as well as by heating it above T_c.

In a typical, small, sample of terrestrial superconductor, T, B, and the mass density ρ will be very close to constant, and once cooled sufficiently, the onset of superconductivity will occur effectively instantaneously and globally throughout the sample. The Meissner effect sets in, with the superconducting electrons forming a supercurrent that screens the interior of the sample from the externally imposed field, and in the simplest case of low temperatures and weak magnetic fields $B < H_c$, the magnetic flux is effectively transported out of the bulk of the sample, into a thin boundary layer. Like the onset of superconductivity, the action of the Meissner effect in expelling magnetic flux is effectively instantaneous, leaving a steady-state solution where the expulsion has been completed. Really, although the term 'Meissner expulsion' has connotations of the process of field rearrangement itself, there is no 'Meissner term' that can simply be inserted into Ohm's law and thence into Faraday's equation to describe the evolution of the field during this phase. Instead, the expression 'Meissner effect' is used to mean the final state once field rearrangement is over, where the free energy is minimized. This endpoint can be readily calculated, from the London equation for a magnetic field $\boldsymbol{B}$ in equilibrium:

$$\nabla^2 \boldsymbol{B} = \frac{\boldsymbol{B}}{\lambda^2}. \tag{1}$$

The solution to this is a magnetic field that drops exponentially from its external value to zero inside the medium, over a length-scale λ known as the penetration depth, which is in good agreement with experimental studies. Though the final Meissner state is simple, a literature review indicates that the very brief phase of flux rearrangement prior to the realization of this state is not a research priority for the field of terrestrial superconductivity, neither for experimentalists nor theorists. It has even been argued that the standard theory of superconductivity is not actually able to explain the dynamics leading to Meissner expulsion (Hirsch 2012).

In contrast to the terrestrial case, the onset of superconductivity and the Meissner effect are slow processes for an NS. T_c depends on ρ, which in turn varies by a factor of up to ~ 10 in an NS core. Because the core evolves into a roughly isothermal state before the first onset of superconductivity, the variation in T_c throughout the core directly corresponds to variation in the time at which different layers become superconducting. Neither the density profile of the core, nor the critical temperature, are known to a high degree of certainty, as a result of differing approaches to treat the relevant microphysics – but the qualitative details are quite robust (Sedrakian & Clark 2019), and are as follows. The first thin shell of superconducting matter forms in the outer core at some radius $\mathcal{R}$, not far in from the crust–core boundary, some minutes after the star's birth. The shell becomes thicker, expanding both inwards and outwards on the cooling timescale for the star; it reaches the crust–core boundary quickly, but its inward progress is slower. Here, the evolution may differ from model to model, depending on the equation of state and gap model, and in some cases the superconducting region may still not have reached the centre after 10^6 yr (Ho, Andersson & Graber 2017); though for some of the models presented here, the inner part of the T_c profile may be irrelevant, as the inward progress of the superconducting shell can be arrested by a core region of magnetic field amplified to the critical field strength (see Section 5). Note that the core neutrons will also undergo pairing, forming a superfluid, but at a substantially lower critical temperature of $\sim 5 \times 10^8$ K (Page et al. 2011), corresponding to a stellar age of ~ 300 yr; we will therefore treat them as a normal fluid throughout this paper.

We will use a single critical temperature and cooling model here for simplicity, but clearly the analysis could be repeated for any other equation of state and gap model, were there motivation to do so. In particular, following Ho, Glampedakis & Andersson (2012), we use an approximation to the proton pairing gap of Chen et al. (1993), parametrized in terms of the particle number density, which can then be rewritten to give T_c as a function of ρ (multiplying the number density by the average nucleon mass). Converting this into an expression for T_c as a function of radius requires us to specify a density profile for the star, i.e. an equilibrium solution for a particular equation of state. An obvious simple choice would be the analytic solution from the Lane–Emden equation for an $N = 1$ polytrope, for which the density profile is

$$\rho(r) = \rho_c \operatorname{sinc} \xi \;\; ; \;\; \xi = \frac{\pi r}{R_*}, \tag{2}$$

where ρ_c is the central density. However, although we will employ this later for an analytic expression for a magnetic-field equilibrium (for which, we will argue, it is quite accurate), for the calculation of T_c it results in a rather unrealistic profile. Instead, we find that a tweak to equation (2) gives a profile very close to that of the SLy equation of state (Douchin & Haensel 2001) for densities above the crust–core boundary value $\rho_{\rm cc} = 1.4 \times 10^{14}\,{\rm g\,cm^{-3}}$ (which is the only part of the profile relevant here):

$$\rho(r) = \rho_c \sqrt{\operatorname{sinc}(1.06\xi)}. \tag{3}$$

Of course this expression is of no significance in the context of the Lane–Emden equation – it is just a convenient closed-form expression that emulates a realistic core equation of state. The critical temperature also depends on the proton fraction x_p. Following Glampedakis, Andersson & Lander (2012), we assume a simple linear dependence on ρ:

$$x_p = 0.1 \frac{\rho}{\rho_c}. \tag{4}$$

Utilizing these results, and with the parametrization of Ho et al. (2012), we are able to produce a critical-temperature profile.

Finally, to track the spreading of the superconducting region over time as the core temperature drops, we use the closed-form cooling prescription for an isothermal core of Page, Geppert & Weber (2006), employing values for the completely unpaired case (recalling that neutrons, representing the bulk of the star's mass, are normal at this stage). Comparing this with the T_c profile, we find that the onset of superconductivity happens after 170 s and at a radius of $r/R_* = 0.79$. The spreading of the superconducting region then proceeds as shown in Fig. 1.

The aim of this paper is to consider possible scenarios by which the Meissner effect is realized in an NS, over the long phase during which the region of superconductivity spreads to encompass most of the core. We will argue that whether or not the magnetic field can be rearranged to realize the Meissner effect depends on processes occurring just as a first thin shell drops below T_c. The first process involves fluid motions at the onset of superconductivity which, through Alfven's frozen-flux theorem, drag field lines around; the second is the subsequent process of magnetic reconnection that causes sufficiently distorted field lines to pinch off and separate. If either process is ineffective the Meissner state will not be realized, even though it is the state minimizing the free energy of the system for $B < H_c$. The field configuration resulting from this first phase then dictates the later evolution of the magnetic field in the face of a spreading region of superconductivity.

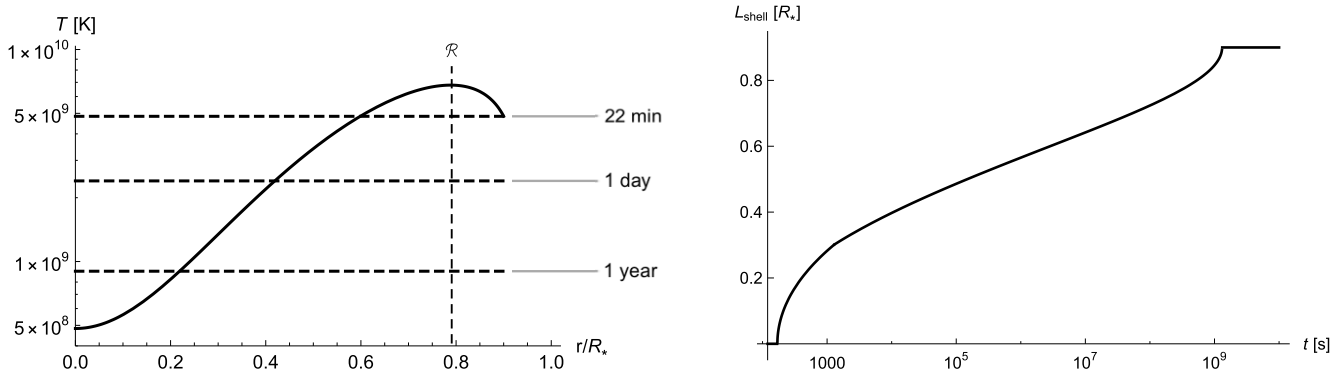

Figure 1. Left: critical temperature for proton superconductivity, using an approximate model similar to that of Ho et al. (2012). Assuming an isothermal core cooling according to the approximation of Page et al. (2006) and overlaying these (horizontal) lines for different ages, we find that the first thin shell of superconducting matter forms after 170 s at the dimensionless radius marked $\mathcal{R}$, and the superconducting shell reaches the crust–core boundary after 22 min. A few other ages are shown, and in the absence of magnetic field the entire core will become superconducting after 42 yr. Right: thickness of the superconducting shell, as a fraction of the stellar radius R_*, as a function of time t.

3 FIELD REARRANGEMENT AT THE ONSET OF SUPERCONDUCTIVITY

What happens when the first superconducting shell forms will dictate the later magnetic-field structure, so this is a logical place to start any analysis.

3.1 Time-scales

The likely slow nature of Meissner expulsion from a superconducting NS core was discussed in the landmark paper of Baym, Pethick & Pines (1969a), who identified the process with that of Ohmic decay:

$$\frac{\partial \boldsymbol{B}}{\partial t} = -\frac{1}{4\pi}\nabla \times \left(\frac{c^2}{\sigma}\nabla \times \boldsymbol{B}\right) \tag{5}$$

with characteristic time-scale

$$\tau_{\rm Ohm} = \frac{4\pi\sigma l_{\rm char}^2}{c^2}, \tag{6}$$

where σ is the electrical conductivity and $l_{\rm char}$ some characteristic length-scale for the magnetic field. This implicitly assumes that the mechanism for transporting magnetic flux in order to achieve Meissner expulsion must be a dissipative one. But NS core matter – in its normal state – forms an outstandingly good electrical conductor, leading Baym et al. (1969a) to conclude that field expulsion would proceed on a time-scale comparable with the age of the Universe. This assertion has been reported uncritically ever since, but – as we have already noted – the condensation of the core protons into a superconducting state is itself very slow and may never be completed, so clearly one cannot make estimates for the whole core in this manner. The spreading of the superconducting region occurs on the cooling time-scale, and is of great relevance, since it may be ongoing in at least the younger observed NSs, and could have important observational consequences. The only study to date that explores this time-dependent process appears to be that of Ho et al. (2017). These authors make a significant new contribution to the problem: a detailed comparison of the shortest magnetic-field evolutionary time-scales (which they find to be Ohmic decay and the drag due to scattering of electrons against flux tubes) with the cooling time-scale. From this they find that the cooling time-scale is always shorter than that of field evolution, until a temperature of $T < 10^8$ K (equivalently, an age $\gtrsim 10^6$ yr), and therefore that in any NS hotter (younger) than this, flux expulsion is not possible.

What these earlier studies and others all have in common is the association of a Meissner-type expulsion from a region of the star with decay of the magnetic field there, but the Meissner effect is not itself instrinsically dissipative. In fact, as noted earlier it is not an evolutionary process at all, but just a statement about the system's desired minimum-energy equilibrium configuration (in its simplest form, it is found as a solution to the time-independent London equation 1).

Here, we build on the arguments of Ho et al. (2017), but argue that the shortest relevant magnetic-field time-scale is not due to either of the secular dissipative effects they invoke, but rather the dynamical time-scale associated with the advection of magnetic field by the fluid flow. This evolution is given by the expression

$$\frac{\partial \boldsymbol{B}}{\partial t} = \nabla \times (\boldsymbol{v} \times \boldsymbol{B}), \tag{7}$$

where the velocity could, in principle, be approximately as high as the Alfvén speed $v_A = B/\sqrt{4\pi\rho}$. Here, we are interested in the fastest possible evolution, so we set $|v| = v_A$, leading to a characteristic dynamical time-scale

$$\tau_A = \frac{l_{\rm char}}{v_A} = \frac{l_{\rm char}\sqrt{4\pi\rho}}{B} = 35\, l_{\rm char,6}\rho_{14}^{1/2}B_{12}^{-1}\ {\rm s}, \tag{8}$$

where we have employed the short-hand notation that a numerical subscript n on a variable means its value in cgs units divided by 10^n, e.g. $l_{\rm char,6} = l_{\rm char}/(10^6\,{\rm cm})$. In equation (8), τ_A is vastly shorter than flux-dissipation time-scales, but the comparison with the cooling time-scale $\tau_{\rm cool}$ is equivocal. Taking, for example, the result from Page et al. (2006) for slow neutrino cooling (i.e. indirect Urca processes) in the absence of any Cooper-pairing, and using their fiducial values for heat capacity and the temperature–luminosity relation, we have

$$\tau_{\rm cool} \approx 3 \times 10^6\, T_9^{-6}\ {\rm s}. \tag{9}$$

Evaluating this for the peak critical temperature from before, $T_9 = 6.8$, gives $\tau_{\rm cool} = 30$ s – identical (to the level of approximation) to the pre-factor from equation (8) for τ_A, and presaging our later conclusions that the efficacy of the Meissner effect depends quite sensitively on the strength and characteristic length-scale of the magnetic field at the onset of superconductivity.

We will explore this dynamical Meissner process in detail, regarding it as one that achieves flux expulsion mostly through field rearrangement, rather than a wholesale dissipation of flux.

3.2 Restrictions

However the Meissner effect proceeds, it has to obey some basic rules (Mestel 2012). First, by integrating the Maxwell equation $\nabla \cdot \boldsymbol{B} = 0$ over the volume enclosed by the initial superconducting shell at radius $r = \mathcal{R}$ and converting it to a surface integral over this shell, we see that the magnetic field normal to the surface $B_\perp$ must be continuous across this surface:

$$\begin{aligned} 0 &= B_\perp^{\rm in} - B_\perp^{\rm out} \\ &= B_r^{\rm in} - B_r^{\rm out} \quad \text{for a spherical surface } r = \mathcal{R}. \end{aligned} \tag{10}$$

This result is universal, and so no evolution mechanism can simply 'cut' and rejoin radial field lines across the initial shell of superconductivity in order to effect flux expulsion. That is, even in the previously considered idea of flux expulsion via dissipation, it is not enough for Ohmic decay simply to reduce the overall magnetic-field strength across the superconducting shell – it must qualitatively rearrange it too.

Secondly, we define the magnetic flux through a surface S:

$$\begin{aligned} \mathfrak{F} &\equiv \int \boldsymbol{B} \cdot \mathrm{d}\boldsymbol{S} = \int B_\perp \, \mathrm{d}S \\ &= \int B_r \, \mathrm{d}S_r = \mathcal{R}^2 \int B_r(\mathcal{R}, \theta, \phi) \sin\theta \, \mathrm{d}\theta \mathrm{d}\phi \\ &\quad \text{for a spherical surface } r = \mathcal{R}. \end{aligned} \tag{11}$$

In the ideal MHD limit, $\mathfrak{F}$ must be conserved during the advection of field lines by the fluid, i.e.

$$\frac{\partial \mathfrak{F}}{\partial t} = 0 \Rightarrow \mathfrak{F}_{\rm in} = \mathfrak{F}_{\rm out} = \mathfrak{F}_0, \tag{12}$$

where $\mathfrak{F}_{\rm in}$, $\mathfrak{F}_{\rm out}$, and $\mathfrak{F}_0$ are, respectively, the magnetic flux across the inner and outer boundaries of the superconducting shell, and across the shell of radius $r = \mathcal{R}$ just prior to the onset of superconductivity. This will be exactly satisfied for the dynamical-time-scale process of dragging field lines around by the fluid, and very well satisfied for almost all of the epoch during which the superconducting shell expands, given that the cooling time-scale is almost certainly considerably shorter than the Ohmic decay time-scale. The one exception, where a significant change in $\mathfrak{F}$ may occur on short time-scales, is if there is a phase of magnetic reconnection across the newly formed superconducting shell.

3.3 Pre-condensation field configuration

To gain any detailed understanding of how much the Meissner effect acts, we need a quantitative model of the magnetic field B_0 immediately prior to the first onset of superconductivity. Without this we cannot make any predictions, since time-scale and energy considerations both involve the characteristic length-scale and distribution of the magnetic field. The restrictions (10) and (12) will also have different implications for different field geometries. For example, one could imagine a contrived initial field configuration that just so happens to have $B_\perp = 0$ all along the spherical shell at which superconductivity first sets in – i.e. there are no field lines crossing the shell. Neither of the two earlier restrictions applies, and as the superconducting shell expands it is able just to push the outer zone of the field further outwards, and the inner zone further inwards; it can thus straightforwardly realize a complete Meissner expulsion. This field configuration is, however, a pathological case: a poloidal field would never naturally have such a geometry because, among other reasons, the radius $r = \mathcal{R}$ is of no physical significance to the pre-condensed state of the star.

On the other hand, every purely toroidal field has the property of no field lines crossing $r = \mathcal{R}$, potentially allowing for a straightforward expulsion from the growing superconducting region (see later discussion, in Section 6.1). There are, however, two strong arguments to dismiss toroidal fields as generic models for an NS field: first, all their field lines close within the star, leaving $B = 0$ outside and rendering the object undetectable as a typical NS; secondly, such field configurations are dynamically unstable (Tayler 1973) and so could not be long-lived.

In fact, the second argument against purely toroidal fields also applies to purely poloidal fields: they suffer instabilities on dynamical time-scales and so will not be realized in nature (Wright 1973), meaning that any realistic field configuration must contain both toroidal and poloidal components, whose exact form will not be generic but rather determined by the birth dynamo that amplifies the field, together with early-time dynamics and stability. However, for the purposes of this paper the most important feature of any realistic pre-condensation field configuration is that there will always be field lines crossing the initial superconducting shell. Now, without any straightforward route to a Meissner-expelled state, the magnetic-field evolution will involve the interplay between the superconducting region wanting to realize its minimum-energy state, and the energy penalty associated with stretching and breaking field lines in order to realize such a state.

We wish to start with the simplest non-trivial, realistic, pre-condensation field configuration, and one we can progressively build upon to increase the level of realism. For this, we will take an axisymmetric, purely poloidal, dipolar, magnetic field. This case embodies the basic and most important feature for our analysis: that magnetic-field lines will always cross the nascent superconducting shell. If one understands this test case, then we argue later on (Section 6.1) that more realistic, complex field geometries – featuring higher multipoles, a toroidal component, a non-axisymmetric structure – can be tackled incrementally, and do not pose specific new conceptual challenges.

We will also assume that the magnetic field is weak enough so that the minimum energy state is full flux expulsion (regardless of whether the star can actually achieve this). Quantifying the strength of a 'weak' field warrants a brief digression. We first remark that different regions of an NS may harbour protons with different superconducting properties, known as type-I or type-II superconductors. We will not discuss the differences in detail here (although see e.g. Tilley & Tilley 2019; Glampedakis, Andersson & Samuelsson 2011), since the classification is related to the minimum-energy state of a superconductor in the presence of stronger magnetic fields than those we consider here. We do, however, need to understand the physical meanings of the four critical fields related to these type of superconductivity: these are usually denoted H_{cI}, H_c for type-I superconductivity and H_{c1}, H_{c2} for type-II superconductivity. Two of these fields represent upper limits: superconductivity is destroyed if $B > H_c$ (H_{c2}) for a type-I (type-II) superconductor, meaning the stellar fluid then behaves as in normal MHD. The other two fields are lower limits for flux penetration: if $B < H_{cI}$ (H_{c1}) for a type-I (type-II) superconductor, the minimal-energy state is full flux expulsion. Finally, magnetic fields with strengths between these lower and upper limits will penetrate the superconductor, but through small-scale flux structures rather than the smooth local field distribution expected for normal MHD.

The critical fields for a type-II superconductor depend only on quantities related to the equation of state (Glampedakis et al. 2011),

in particular the proton fraction and the effective proton mass[1] and not the magnetic field itself. The upper critical fields for type-I and type-II superconductors are also related in a simple way, $H_{c2} = \sqrt{2}\lambda H_c/\tilde{\xi}$, where $\tilde{\xi}$ is the proton coherence length. But the lower critical field of a type-I superconductor is geometry-dependent – for example, for a spherical superconductor in a vertical field, $H_{cI} = (2/3)H_c$; in other geometries H_{cI} may be as high as H_c or as low as zero.

The critical fields do not all vary in the same way with the star's density (equivalently, radius), but ignoring the very specific case where H_c drops to zero for the type-I case, the variation in the lower critical fields H_{cI} and H_{c1} will generally only be by a small factor, mainly in the rough range $5 \times 10^{14} - 10^{15}$ G (e.g. Glampedakis et al. (2011)). Our priority is to establish a single, representative, cut-off value below which a magnetic field will be energetically favoured to be expelled from the superconducting region, without needing to change treatment above a certain density, nor for a certain field configuration. Because the variation in lower critical fields is relatively small, we will simply assume a spatially constant critical field, and re-appropriate the symbol H_c to denote this value, remaining agnostic about the type of superconductivity, i.e. by 'weak fields' we mean the case

$$B < H_c \ , \ \text{where } H_c = \text{const} = 5 \times 10^{14}\,\text{G}. \tag{13}$$

Although at least some NSs probably host interior fields $B > H_c$, it will be easier to tackle that case once the weak-field case is better understood. We briefly discuss stronger fields at the end of this paper, but defer any detailed calculations to future work.

3.4 Stretching of field lines during the onset of superconductivity

Having established a representative pre-condensation magnetic field and explored restrictions on how this field can be rearranged, we are now in a position to describe our scenario for realizing a Meissner state on a dynamical time-scale. This scenario consists of two steps: first, distorting the field through advection into a geometry amenable to magnetic reconnection, and secondly, the reconnection phase itself. We consider the first step in this subsection, and the second in the following subsection. The first step envisages a transitional phase between the normal and superconducting phases: that, at the onset of superconductivity, fluid motions (treated with normal MHD) seek to drag the magnetic field into the lower energy state desired by the superconducting shell. To start with, then, we need to understand whether this is plausible.

The minimum thickness for which the incipient shell can display its superconducting properties is given by the penetration depth λ, which for the outer part of the NS core (where superconductivity will first develop) is given by (Mendell 1991)

$$\lambda \approx 10^{-11}\,\text{cm}. \tag{14}$$

Clearly the shell's thickness will expand to a huge multiple of λ almost instantaneously, well within a typical Alfvén time-scale, which by equation (8) is of order seconds. This suggests that long before any fluid motions can act to distort the initial magnetic field, the shell will be firmly in the superconducting phase, invalidating the whole approach of this paper. However, the fact that the incipient superconducting shell is – by definition – at a temperature $T \approx T_c$ changes this conclusion.

[1]See e.g. Chamel (2008) for profiles of these quantities.

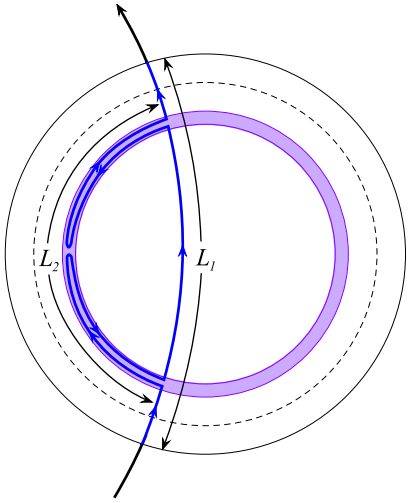

Figure 2. Geometry of a field line distorted from its original length L_1 due to shearing in the incipient superconducting shell (the thick shaded purple circle).

The penetration depth λ and critical field H_c are temperature-dependent, and at temperatures close to T_c differ from their zero-temperature values λ_0, H_{c_0} in the following manner (Tinkham 2004):

$$\frac{\lambda(T)}{\lambda_0} = \left[1 - \left(\frac{T}{T_c}\right)^4\right]^{-1/2} , \ \frac{H_c(T)}{H_{c_0}} = 1 - \left(\frac{T}{T_c}\right)^2 . \tag{15}$$

Consider the state of the star 10 s[2] after the onset of superconductivity. After this time, the superconducting shell has already expanded to $0.05R_*$, i.e. 6×10^4 cm for a 12-km star: likely to be far longer than the characteristic length-scale for any fluid motion (this is discussed more in Section 3.5). The critical temperature at the inner and outer surfaces of the shell is (by definition) exactly equal to the current temperature of the core, whilst within the shell at $r = 0.79R_*$ – the point of first onset of superconductivity – the temperature is 0.96 per cent below its critical value. This corresponds, using the above relations, to a penetration depth 5.2 times longer than λ_0 and a critical field 53 times lower than H_{c_0}. The former modification is clearly not significant (λ remains vastly shorter than any relevant hydrodynamic length-scale), but the latter is dramatic. Taking our fiducial value of $H_{c_0} = 5 \times 10^{14}$ G, it would mean that the $0.05R_*$-thick superconducting shell would have a critical field no higher than 10^{13} G in its centre, and lower towards its boundaries. Given that the shell need not be this thick before field rearrangement occurs, $H_c(T)$ would be even lower and very likely weaker than the existing field in that region; from this we conclude that it is reasonable to treat the early-stage dynamics in the shell with normal MHD.

For a simple dipolar geometry, field lines need to be advected a distance comparable with the stellar radius, i.e. $\approx 10^6$ cm, in order to produce a geometry where reconnection can later occur; see Fig. 2. If the Alfvén speed is too low, this advection will not have time to produce such a geometry before the region is enveloped by the superconducting region. To estimate the characteristic angular length-scale $\mathcal{L}_\parallel$ associated with advection in the incipient shell, we set the Alfvén (8) and cooling (9) time-scales equal to one another for the appropriate values for the onset of superconductivity ($T_9 = 6.8$ and $\rho_{14} = 4.3$) within our model, yielding the result

$$\mathcal{L}_{\parallel,6} \approx 1.3 B_{12}. \tag{16}$$

[2]Chosen for the sake of definiteness; our conclusions do not rely on the specific time.

From this, we conclude that hydromagnetic motions can rearrange the field in the nascent superconducting shell sufficiently (i.e. over a 10^6-cm scale) if the pre-condensation magnetic-field strength

$$B_0 \gtrsim 10^{12}\,\mathrm{G}. \tag{17}$$

Why should these motions set in to start with? First, it is natural to assume that the star is not strictly static; even motions from the star's birth may not have been entirely dissipated by viscosity in that time. Secondly, even if the star had managed to achieve a strict equilibrium with the pre-condensation field, the change of magnetic force from the normal-matter Lorentz force to the corresponding magnetic force for a superconductor would itself be enough to violate the equilibrium and hence induce fluid motion. Thirdly, the condensation energy density

$$\frac{H_c^2}{8\pi} = f_n^0 - f_s^0 \tag{18}$$

represents the difference in Helmholtz free energies at $B = 0$ for the superconducting f_s^0 and normal f_n^0 states,[3] so that the Meissner state is able to minimize free energy, even though it will involve distorting field lines away from the pre-condensation state, and thus increasing the overall magnetic energy (Annett 2004).

The detailed dynamics will inevitably be complex and are beyond the scope of this first analysis, and we will just assume that they act to drive the magnetic field in the superconducting region towards its minimum-energy state of full expulsion. We come back to this point in Section 7.

Fluid motions that stretch the field lines also increase the total magnetic energy of the configuration, and for full Meissner expulsion the fluid would need to advect the field lines in such a way as to bunch them all up in a very small volume of the superconducting shell, where they are highly distorted, have a small local characteristic length-scale, and hence are susceptible to reconnection. Reconnection pinches the field lines off across the shell and allows for complete Meissner expulsion, as discussed in the following subsection; for this process, we need to invoke Ohmic decay. But first we consider the case of gradually distorting the magnetic-field lines, when the characteristic length-scale is still too long to need to worry about dissipative effects, and we can assume infinite conductivity of the matter, with the field lines perfectly frozen into the fluid.

Consider an infinitesimally thin flux tube of cross-sectional area $\mathrm{d}A$ running along the entire interior length L_1 of a magnetic-field line, before the onset of superconductivity. It is likely safe to assume, to leading order, that any internal distortion of the field line will have no effect on the part of the field line that extends outside the star, and so we may ignore the exterior field throughout this calculation. We define the magnetic energy of the flux tube $\mathfrak{E}_{\mathrm{mag}}$ as the (field) line integral of the magnetic-energy density $B^2/8\pi$, multiplied by $\mathrm{d}A$:

$$\mathfrak{E}_{\mathrm{mag}} = \mathrm{d}A \int_{L_1} \frac{[B(s)]^2}{8\pi}\,\mathrm{d}s, \tag{19}$$

where s is a parameter defining distance along a field line.

Now assume that the action of fluid motions causes maximal distortion of the (still single) field line, dragging it towards the equator within the superconducting shell, as shown in Fig. 2. When the field line is thus distorted, it gains an additional length $2L_2$ – one factor of L_2 each for its journey towards the equator, and back again. Denoting the radius at which the superconducting shell first appears by $\mathcal{R}$, the length L_2 must be in the interval

$$0 \le L_2 \le \pi\mathcal{R}, \tag{20}$$

and the total length after reconnection is the sum of the lengths of the now-separated two field lines, i.e. $L_1 + 2L_2$. The flux tube energy also gains an additional piece from the stretching, with the total now being related to the sum over the line integrals along both L_1 and L_2:

$$\mathfrak{E}_{\mathrm{mag}} = \mathrm{d}A \left(\int_{L_1} \frac{[B(s_1)]^2}{8\pi}\,\mathrm{d}s_1 + 2\int_{L_2} \frac{[B(s_2)]^2}{8\pi}\,\mathrm{d}s_2 \right), \tag{21}$$

where the two parametrizing functions s_1 and s_2 may be different.

This increase in magnetic energy must be sourced from somewhere, be it kinetic energy from residual fluid motion remaining from the birth phase, the condensation energy, or any other physics related to the onset of superconductivity. It is certainly unlikely that the star will be entirely static, so there may be a substantial well of kinetic energy to draw upon, but there is no obvious way to quantify this whilst retaining the generality of the model. Instead, as an indicative upper limit on how much the field can be distorted, we will regard the magnetic energy increase as being sourced solely by the condensation energy in the relevant superconducting shell. Calculating this is problematic, since (unlike terrestrial calculations) it is not obvious what volume of shell to use, and because within this shell $H_c(T)$ could be substantially lower than the zero-temperature value we mean when we write H_c. To give ourselves an order-of-magnitude idea of the kind of well of energy we may be able to draw on, we estimate the condensation energy using the zero-temperature $H_c = 5 \times 10^{14}\,\mathrm{G}$ and a shell extending from $0.8 - 0.9R_*$:

$$\int_{\mathrm{shell}} \frac{H_c^2}{8\pi}\,\mathrm{d}V \approx \frac{4\pi[(0.9R_*)^3 - (0.8R_*)^3]}{3}\frac{H_c^2}{8\pi} \sim 10^{46}\,\mathrm{erg}, \tag{22}$$

assuming a stellar radius $R_* = 12\,\mathrm{km}$.

This suggests – somewhat counterintuitively – that Meissner expulsion from the superconducting region actually increases the total magnetic energy of the star, at least in the initial field-line-stretching phase; we can get a qualitative estimate of this increase by assuming the stretching roughly doubles the average length of field lines (based on the sketch of Fig. 2), and therefore also roughly doubles the magnetic energy. Some, and possibly most, of this additional energy will be lost if there is a reconnection phase afterwards; we will make quantitative calculations of these values for a specific model in the following section.

Finally, we recall that Meissner expulsion represents the system seeking a lowest energy state where $B = 0$, and so is not expected unless $B \lesssim H_c$. Essentially, the same physics is also encapsulated by the requirement that any field-line stretching increases the magnetic energy by at most the estimate of equation (22).

3.5 Resistivity and reconnection

We assume that the main cause of flux rearrangement during the onset of superconductivity is due to advection by fluid motions, with the field being perfectly frozen into the fluid, as is the case where the conductivity is infinite. Through this process, the field lines in the thin initial shell of superconducting matter could be dragged around significantly; see Fig. 2 and the middle row of cartoons from Fig. 3. However, Meissner expulsion can not be completed unless the highly sheared magnetic-field lines ultimately reconnect. We assume the matter can still be treated as in a normal state here, since reconnection should occur (if it occurs) at the onset

[3]This expression is for the condensation energy at zero temperature; the energy will be substantially smaller close to T_c.

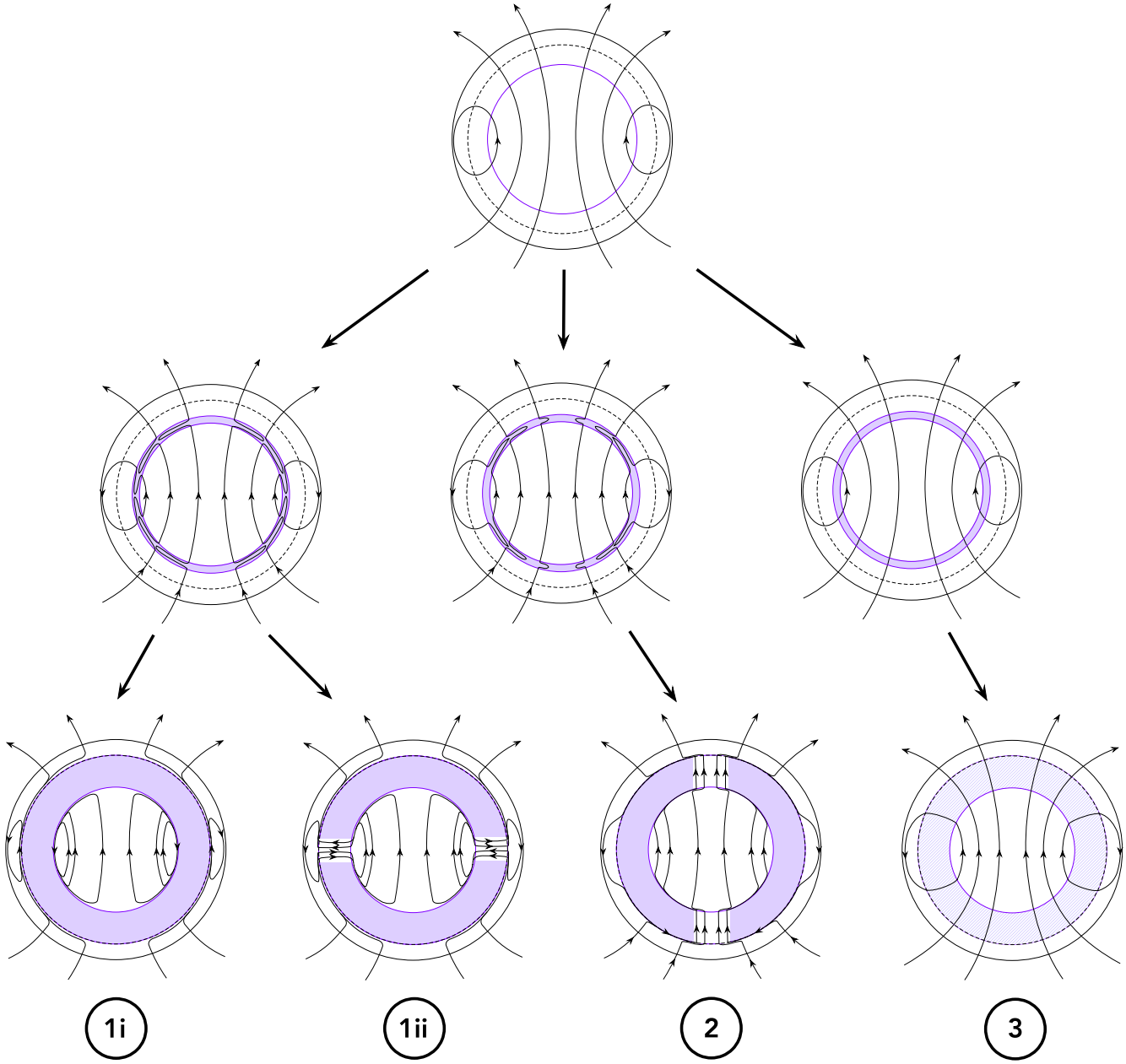

Figure 3. Four different scenarios for the rearrangement of flux due to the expanding region of superconductivity, all for $B < H_c$. An initially dipolar poloidal magnetic field (top row) may be advected by fluid motions (middle row) and then experience reconnection (bottom row). The (in)efficacy of these processes leads to four post-condensation field configurations.

of superconductivity, when $T \approx T_c$ and $B > H_c(T)$, as discussed in the previous subsection. Even if there is significant supercurrent screening, however, causing a substantial reduction in the value of B compared with elsewhere in the star, this will not affect the calculation, since neither reconnection nor cooling depend (to leading order) on the magnetic-field strength itself.

Whether the advected field discussed in the previous section can reconnect depends on whether or not this process is faster than the spreading of the superconducting region as the star cools, i.e. the efficacy of reconnection in this scenario can be measured with the ratio:

$$\frac{\tau_{\rm rec}}{\tau_{\rm cool}}. \tag{23}$$

The smaller the value of this ratio, the more efficiently reconnection should be able to alter the geometry of the distorted field in the thin shell where superconductivity begins. Amongst the various mechanisms for magnetic reconnection in the literature, there are essentially two kinds of relevance here; both are related to Ohmic decay (and so depend upon the resistivity of NS matter in its normal state), but they differ in the assumed characteristic magnetic-field length-scale and small-scale magnetic-field structure. The first is the classic Sweet–Parker reconnection (Parker 1957; Sweet 1958), which acts on the macroscopic field; the second is stochastic reconnection, frequently invoked to explain the phenomenon of fast dynamo action in stars (Lazarian & Vishniac 1999), where jagged microscopic field structures allow for a faster diffusive rearrangement of magnetic field.

We begin with the Sweet–Parker mechanism, whose reconnection time-scale is simply that of Ohmic decay, $\tau_{\rm rec} = \tau_{\rm Ohm}$. To evaluate this, we adopt the density- and temperature-dependent expression for σ from Baym et al. (1969b), together with our previous approximation (4) for proton fraction, which gives us

$$\sigma = 4.7 \times 10^{26}\, \rho_{c,15}^{-3/2} \rho_{15}^{3} T_{10}^{-2}\, {\rm s}^{-1}. \tag{24}$$

Now plugging this into equation (6) and using the cooling prescription of Page et al. (2006), we arrive at the ratio

$$\frac{\tau_{\rm rec}}{\tau_{\rm cool}} = 2.2 \times 10^{6} \rho_{c,15}^{-3/2} \rho_{15}^{3} T_{10}^{4} l_{\rm char,1}^{2}. \tag{25}$$

The large pre-factor suggests that Sweet–Parker reconnection is unlikely to be effective at flux rearrangement at the onset of superconductivity, given the plausible range in which the other quantities can vary. For our particular model, the onset of superconductivity occurs at $T = 6.8 \times 10^{9}$ K and at a radius $0.79 R_{*}$, which corresponds to a density $\rho_{15} = 0.43$ for a model with central density $\rho_{c,15} = 1$. Let us insert these values into equation (25), and also change notation from $l_{\rm char}$ to $\mathcal{L}_{\perp}$, to emphasize the fact that the relevant length-scale is related to the component of the magnetic field/fluid motion normal to the nascent shell of superconductivity (cf. equation 16 for $\mathcal{L}_{\parallel}$):

$$\frac{\tau_{\rm rec}}{\tau_{\rm cool}} = 3.7 \times 10^{4} \mathcal{L}_{\perp,1}^{2}, \tag{26}$$

i.e. that only a characteristic field length-scale $\mathcal{L}_{\perp} \lesssim 10^{-3}$ cm would allow for effective reconnection. A large-scale configuration like a dipolar field, with $\mathcal{L}_{\perp} \sim 10^{6}$ cm, will therefore clearly not experience any qualitative rearrangement on the onset of superconductivity. If field lines are, however, strongly distorted in the initial shell of superconductivity, the length-scale becomes shorter. Determining this length-scale quantitatively requires a full, numerical, solution of the MHD equations for this scenario, but we can at least determine a minimum characteristic length-scale. This will depend on whether the main dissipative mechanism acting on the MHD flow is due to resistivity $c^{2}/(4\pi\sigma)$ or viscosity ν.

Although the NS is only 170 s old, it is still comfortably in the neutrino-transparent phase (Burrows & Lattimer 1986), for which viscosity is dominated by the contribution from neutron–neutron scattering (Flowers & Itoh 1979), with (Cutler & Lindblom 1987)

$$\nu \approx 19\, \rho_{15}^{5/4} T_{10}^{-2} {\rm cm}^{2}\, {\rm s}^{-1}. \tag{27}$$

At the onset of superconductivity in our model, this gives a value of $\nu \approx 10\, {\rm cm}^{2}\, {\rm s}^{-1}$. We can now combine equations (24) and (27) to yield an expression for the magnetic Prandtl number Pm, the ratio of resistivity to viscosity:

$${\rm Pm} = 1.2 \times 10^{8}\, \rho_{c,15}^{-3/2} \rho_{15}^{17/4} T_{10}^{-4}. \tag{28}$$

At the onset of superconductivity this gives ${\rm Pm} = 1.6 \times 10^{7}$, and shows that the shortest characteristic length-scale will be set by the viscosity, which acts on a fluid flow that can be no faster than the Alfvén speed $v_{A} = B/\sqrt{4\pi\rho}$; now combining ν and v_{A} and with suitable parametrizations, we arrive at a lower limit for the characteristic length-scale of the viscous MHD flow:

$$l_{\rm visc} = \frac{\nu\sqrt{4\pi\rho}}{B} = 2.1 \times 10^{-3}\, \rho_{15}^{7/4} B_{12}^{-1} T_{10}^{-2}\, {\rm cm}. \tag{29}$$

Inserting values for the onset of superconductivity, within the model we adopt, yields a viscous scale of

$$l_{\rm visc} = 1.1 \times 10^{-3} B_{12}^{-1}\, {\rm cm}. \tag{30}$$

Reconnection cannot proceed if it requires a shorter length-scale than $l_{\rm visc}$, so we compare the latter with the $l_{\rm char}$ required to produce a ratio of unity in equation (25): this shows that for Sweet–Parker reconnection to be at least marginally effective, it requires

$$B_{0} \gtrsim 10^{12}\, {\rm G}. \tag{31}$$

This only proves that this reconnection scenario is not implausible for a maximally distorted pre-condensation field $\gtrsim 10^{12}$ G; only simulations can determine whether it is actually likely. Note that Meissner expulsion through the mechanism discussed in this paper requires both significant advection of the fluid flow and effective reconnection, and these lead to identical minimum-field requirements, equations (17) and (31), respectively. This is just a coincidence, but it does make the lower field bound more robust.

Next we examine the mechanism of stochastic reconnection. This mechanism has proved invaluable in understanding the problem of fast dynamos in astrophysics, i.e. dynamos whose field-amplification rate becomes independent of resistivity in the limit of vanishing resistivity. The original work on this topic gives a reconnection speed $v_{\rm rec}$ that depends upon the rms velocity due to energy injection at the stochastic scale v_{T}, and upon the ratio of two key length-scales, the width of the reconnection region L_{x} and the scale of energy injection $l_{\rm inj}$ (Lazarian & Vishniac 1999):

$$v_{\rm rec} \lesssim v_{T} \min\left\{ \sqrt{\frac{L_{x}}{l_{\rm inj}}}, \sqrt{\frac{l_{\rm inj}}{L_{x}}} \right\}, \tag{32}$$

with (as required by the motivation of understanding fast dynamos) no dependence on σ. This expression depends on details of the energy injection, but an indicative range of values for the reconnection speed is $v_{\rm rec} = (0.01 - 0.1) v_{A}$ (Kowal et al. 2009).

The above result is valid when viscosity is weak, which encompasses most astrophysical fluid settings where dynamos and field rearrangement are expected, but we just saw that NSs are an exception to this, with ${\rm Pm} \gg 1$. In this large-Pm regime, the previous reconnection speed is modified to (Jafari et al. 2018):

$$v_{\rm rec} \lesssim v_{T} \frac{L_{x}}{l_{\parallel}} \frac{{\rm Re}^{1/4} {\rm Pm}^{-1/2}}{1 + \ln({\rm Pm})}, \tag{33}$$

where $l_{\parallel}$ is a parallel eddy length-scale. Note that in this case reconnection is no longer truly 'fast', as it regains an implicit dependence on resistivity through the Pm terms. The two length-scales in this relation are not likely to be independent of one another, as both relate to the field structure produced by the MHD flow and therefore should scale with (or be equal to) the viscous scale; we will therefore just pessimistically assume the ratio $L_{x}/l_{\parallel}$ to be unity, though it could be substantially larger. For the rms velocity we assume $v_{T} = 0.01 v_{A}$, and we calculate the Reynolds number based on a flow moving at v_{A}, giving ${\rm Re} = 1400\, B_{12} l_{\rm char,1}$. Then, evaluating the ratio in the above expression, we arrive at a stochastic reconnection speed (reduced by viscosity) of

$$v_{\rm rec} = 0.012\, B_{12}^{5/4} l_{\rm char,1}^{1/4}\, {\rm cm}\, {\rm s}^{-1}. \tag{34}$$

The ratio of reconnection to cooling time-scales in this case, for our fiducial model parameters for the onset of superconductivity, is therefore

$$\frac{\tau_{\rm rec}}{\tau_{\rm cool}} = 3 B_{12}^{-5/4} l_{\rm char,1}^{3/4}. \tag{35}$$

Although this has a far smaller pre-factor than for Sweet–Parker reconnection (equation 25), this is counteracted by the weaker dependence on $l_{\rm char}$, and setting the above ratio equal to unity indicates that the stochastic reconnection mechanism is effective on somewhat less fine magnetic-field structures than Sweet–Parker reconnection, $l_{\rm char} \lesssim 0.2 B_{12}^{5/3}$ cm. This length-scale is also more comfortably above

the viscous scale (equation 30), at a field strength $B_{12} = 1$. This calculation could therefore be invoked to push the lower limit for partial/complete Meissner expulsion below 10^{12} G – however, given the crude assumptions we have made about parameters related to stochastic reconnection, and the fact that the work of Jafari et al. (2018) was doubtless never intended for the kinds of extreme magnetic Prandtl numbers we consider here, we find it safer to retain 10^{12} G as an indicative lower limit.

To summarize, understanding the role of reconnection at the onset of superconductivity is hampered by the complexity of the process, even with the simplification that it occurs in normally conducting matter. Sweet–Parker reconnection involves one characteristic length-scale; stochastic reconnection involves at least two – and none of these can be satisfactorily analysed without simulations. We can however draw some useful conclusions. MHD flows in the high-Pm regime expected in a young NS are capable of producing field structures on a length-scale where reconnection can take place. Furthermore, if the average field strength $B \gtrsim 10^{12}$ G, then reconnection is faster than cooling; the field may be rearranged before the superconducting shell spreads too far. Weaker fields will not be substantially rearranged; for stronger fields, the efficacy of reconnection increases roughly linearly with field strength.

3.6 Four limiting cases

From the previous two subsections, we saw that the range of field strengths for which a partial or complete Meissner expulsion could occur is limited to

$$10^{12}\,\mathrm{G} \lesssim B_0 \lesssim 5 \times 10^{14}\,\mathrm{G}, \tag{36}$$

but that even within this range, expulsion depends on the fluid flow and reconnection properties of the star at the point of formation of the incipient superconducting shell. It is therefore now instructive to consider four limiting cases of how the magnetic field may be affected, and to examine the circumstances under which they may be realized. The final field configuration depends on the efficacy of both field-line advection and the subsequent magnetic reconnection. These four scenarios are summarized in Fig. 3.

In the first scenario for the phase of field rearrangement, fluid motions are effective at transporting the magnetic flux in the superconducting shell to a small equatorial volume of the shell. In the second scenario, there is also large-scale fluid motion, but this time, it advects field lines towards the north and south poles. Finally, the last scenario (scenario 3) accounts for the possibility of negligible fluid motion, and so the field lines remaining undistorted as they cross the superconducting region.

After the advective phase, any reconnection then occurs. In scenario 1, the flux has been concentrated around the equator, forming an X-point geometry with neighbouring field lines having the opposite sense from one another. If reconnection is effective, such a geometry is able to reconnect fully, with every field line pinching off across the incipient superconducting shell, separating from the part of the field line on the other side and rejoining a line on its own side (scenario 1i). If reconnection is ineffective, the concentration of flux produced in an equatorial band (scenario 1ii) will remain there, threading an otherwise $B = 0$ shell. But if the flux is concentrated around the poles, reconnection cannot be effective, both because neighbouring field lines will not have the opposite sense needed, and because the characteristic length-scale of the field across the shell $\mathcal{L}_\perp$ is too long to experience the requisite dissipation to allow for reconnection. The field must then continue to thread through the superconducting shell in these two polar holes (scenario 2). In scenario 3, like scenario 2, there are no regions with sufficiently distorted field lines to be subject to reconnection; the field lines towards the symmetry axis are already fairly straight, and those around the equator will tend to be 'combed out' by the boundary condition between the normal inner region and the expanding superconducting shell (see Henriksson & Wasserman 2013, for a detailed discussion of this). All these possibilities are plotted in Fig. 3.

Scenario 1i is what is usually understood by the term 'Meissner effect', and is what is implied in magnetic-field evolutions that implement a $B = 0$ inner boundary and call it a 'Meissner boundary condition' (e.g. Hollerbach & Rüdiger 2002; Pons & Geppert 2007). It is sometimes thought to be a consequence of type-I superconductivity, and this is not correct; a type-II superconductor can just as effectively expel flux. However, it clearly requires a particular set of circumstances to arise, even for $B < H_c$ where it represents the minimum-energy configuration, because the physics may not allow for it to be realized. Scenario 3 is the opposite limit: one in which the macroscopic magnetic field is essentially unaffected in both its magnitude and direction by the developing superconducting region, except that the closed-field-line region tends to be pushed out of the core altogether, and into the crust. In our model, all pre-condensation fields $B_0 \lesssim 10^{12}$ or $\gtrsim 5 \times 10^{14}$ G are expected to follow this evolutionary path and end up threading the entire superconducting core, but even with the 'right' initial field, $10^{12}\,\mathrm{G} \lesssim B_0 \lesssim 5 \times 10^{14}\,\mathrm{G}$, scenario 3 is also the likely outcome if there is limited advection of field lines. It is worth noting that equilibrium models for a type-II superconducting core with $B < H_c$ (Roberts 1981; Henriksson & Wasserman 2013; Lander 2014) also resemble this outcome, with no field lines closing within the core itself.

Scenarios 1i and 3 are two extremes: one where field is entirely expelled from the superconducting region, and another where it threads the entire region. Between these two lie a variety of possibilities for flux penetration in distinct, macroscopic regions, with other regions where the field drops to zero; the two limiting cases of this group of configurations are scenarios 1ii and 2.

We have argued that all of the four scenarios are, at the very least, plausible, in that they place requirements on the length-scale and time-scale of dynamics in the incipient shell which can be satisfied for some part of the relevant parameter space. A detailed analysis of the early evolutionary phase proposed here is well beyond the scope of this paper, presenting a mixture of conceptual and computational challenges (e.g. in modelling dynamics and reconnection at the onset of superconductivity). None the less, several aspects of the different scenarios are amenable to calculation, using some generic restrictions from MHD theory together with the notion of a maximum permissible field strength, the critical field. We discuss these next.

3.7 Quantifying scenario geometries

We are able to quantify, to some extent, the field borne from each of our four scenarios, using the rules discussed in Section 3.2. We are now focused on the field just after any field rearrangement and reconnection has taken place, whilst the shell is still thin; this corresponds to the bottom row of configurations in the cartoon of Fig. 3, though the thickness of the superconducting shell there is increased for clarity and should not be taken literally. In general, both the magnetic-field component normal to the superconducting shell $B_\perp$ and the component tangential to the shell $B_\parallel$ will vary with position, in different ways. As sketched in the top panel of Fig. 3, the pre-condensation field appears dominantly radial, i.e. $B_\perp \gg B_\parallel$, but through advection (middle panel), it may generate a substantial

parallel component, resulting in $B_\perp \sim B_\parallel$. Quantifying these effects requires a far more sophisticated analysis than the scope of this work. Instead, for simplicity we will assume that $B_\perp$ is constant across the region of the shell that it penetrates, and that the parallel component in these regions is a fixed fraction of the normal component, i.e.

$$B_\parallel = \zeta B_\perp\,, \quad \zeta = \text{const.} \tag{37}$$

Of the four endpoints, we will start with scenario 2, where the field cannot be fully expelled and reconnection will be ineffective due to the large-length-scale field geometry threading the polar regions of the superconducting shell, with all neighbouring field lines having the same sense. The simplest scenario is that superconductivity minimizes the volume of the $B \neq 0$ region of the shell by squeezing the field lines inwards towards the $\theta = 0, \pi$ axis until the magnetic field is so concentrated that its magnetic energy density reaches that of the critical field, i.e. we are left with two normal-matter holes (one for each pole) in the shell, where

$$\frac{B_\perp^2 + B_\parallel^2}{8\pi} = \frac{(1+\zeta^2)B_\perp^2}{8\pi} = \frac{H_c^2}{8\pi} \Rightarrow B_\perp = \frac{H_c}{\sqrt{1+\zeta^2}}. \tag{38}$$

Given that we do not expect any significant reconnection, let us assume that the magnetic flux through both the inner and outer boundaries of the superconducting shell $\mathfrak{F}_{\rm in}, \mathfrak{F}_{\rm out}$ is equal to the pre-condensation value $\mathfrak{F}_0$; see equation (12). Just after the onset of superconductivity we may approximate the initial radius of onset of superconductivity $\mathcal{R}$ and the inner and outer radii of the superconducting shell $R_{\rm in}, R_{\rm out}$ as all having the same value, and the conservation of flux expression becomes a relation between the normal magnetic-field component before $B_\perp^0$ and after $B_\perp^{\rm post}$ condensation:

$$\mathfrak{F}_0 = 4\pi\mathcal{R}^2 B_\perp^0 = 2\pi\mathcal{R}^2 B_\perp^{\rm post}\, 2\int_0^{\theta_{\rm open}} \sin\theta\, {\rm d}\theta = \mathfrak{F}_{\rm in} = \mathfrak{F}_{\rm out} \equiv \mathfrak{F}_{\rm post}. \tag{39}$$

Combining this result with the preceding equation to eliminate $B_\perp^{\rm post}$ yields an expression for the opening angle $\theta_{\rm pole}$ of the normal 'hole' in the superconducting shell:

$$\theta_{\rm open} = \arccos\left(1 - \frac{\sqrt{1+\zeta^2}B_\perp^0}{H_c}\right). \tag{40}$$

For this scenario, then, $\theta_{\rm pole} = \pi/2$ when the pre-condensation field components are $B_\perp = B_\parallel \approx 3.5 \times 10^{14}$ G – i.e. flux conservation dictates that any field stronger than this must thread the entire initial shell of superconductivity.

Scenario 1ii is similar to that of scenario 2, except that now the field is confined around the equator. Again, superconductivity acts to minimize the volume of the shell where $B \neq 0$, resulting in a single equatorial ring of normal matter, cleaving the superconducting shell into two halves. The only change to the previous calculation is that the limits on the θ-integral must now be changed from $\{0, \theta_{\rm open}\}$ to $\{\theta_{\rm eq}, \pi/2\}$, where $\pi/2 - \theta_{\rm eq}$ is the half-angular thickness of the ring (i.e. the total angular extent is double this, by equatorial symmetry), and the result is:

$$\theta_{\rm eq} = \arccos\left(\frac{\sqrt{1+\zeta^2}B_\perp^0}{H_c}\right). \tag{41}$$

As expected, the same value of magnetic field as for scenario 2, $B_\perp = B_\parallel \approx 3.5 \times 10^{14}$ G, results in magnetic flux threading the entire shell.

Scenario 1i invokes a reconnection event to 'pinch off' all the equatorial field lines and leave an unbroken $B = 0$ superconducting shell. Clearly flux is not conserved during this process; beforehand a general field crossing the radius of onset of superconductivity would be expected to have $B_\perp \sim B_\parallel$ and some flux $\mathfrak{F}_0$, but afterwards $\mathfrak{F}_{\rm in} = \mathfrak{F}_{\rm out} = 0$ and $B_\perp \to 0$ when approaching the superconducting shell from either side, as steps in this component violate $\nabla \cdot \boldsymbol{B} = 0$. $B_\parallel$, on the other hand, is permitted to drop abruptly from its value in a normal domain to zero in the superconducting shell, since steps in this component can be matched with a surface current along the normal-superconducting boundary. Flux conservation and the traction condition on $B_\perp$ do not, therefore, provide any restriction on the geometry of scenario 1i.

Finally, in scenario 3, there is no motion tangential to the shell of onset of superconductivity and so no distortion of field lines away from their pre-condensation state. Once a thin superconducting shell has formed, flux conservation and the traction condition imply that the field lines must thread the entirety of the superconducting region on a macroscopic scale, as they previously threaded that volume when it was normal matter. As the shell thickens, the field lines are thus combed out across the shell: not strictly radial, which would lead to kinks at the inner and outer shell boundaries and so require the existence of surface currents, but with minimal curvature to ensure the whole length of each field line is smooth. On a microscopic scale, however, the flux distribution will differ from the pre-condensation state. The evenly distributed flux in the normal-matter region will become split up into thinner flux structures in the superconducting shell, over a transition region whose thickness is the penetration depth. Depending on the type of superconductivity operative in the shell, the flux structures will either be a predictable Abrikosov lattice of evenly distributed flux tubes with central magnetic-field strength $B = H_{c1}$ surrounded by $B = 0$ matter (type-II superconductivity), or regions with various possible thicker (but still small-scale) flux structures with $B = H_c$ alternating with $B = 0$ regions. These two states are the favoured, minimum-energy, states for flux penetration when $H_{cI} < B < H_c$ (type-I superconductivity) or $H_{c1} < B < H_{c2}$ (type-II superconductivity), whereas for the weaker fields we consider here, the global minimum energy state would be a complete shell of $B = 0$. For this region, our scenario 3 represents a state that is sometimes dubbed 'quasi-stable', but we would argue that there is no need for the qualifying prefix 'quasi': it is simply stable, being a local minimum-energy state from which there is no feasible route for the system to reach the $B = 0$ global minimum. We believe this to be a more solid argument than earlier ones (e.g. Baym et al. 1969a) for why an NS with a relatively weak field has flux penetrating the entire core rather than exhibiting the Meissner effect.

3.8 Energy release during reconnection

Let us denote the pre-condensation magnetic energy as $\mathcal{E}_{\rm mag}^0$, and use $\mathcal{E}_{\rm mag}^{\rm str}$ to denote the additional magnetic energy gained from the stretching of field lines in the initial shell of superconductivity. Since in practice we will never be able to 'measure' the pre- or post-condensation magnetic energies, the more relevant quantity is the fractional change α in magnetic energy resulting from the advection of field lines at the onset of condensation, i.e.

$$\alpha \equiv \frac{\mathcal{E}_{\rm mag}^{\rm str}}{\mathcal{E}_{\rm mag}^0}. \tag{42}$$

Reconnection takes a magnetic field from a higher energy configuration to one of lower energy, so this process always releases energy; we will assume this is some unknown fraction β of the energy gained during the advection phase $\mathcal{E}_{\rm mag}^{\rm str}$. How much depends on various factors such as how extensive field-line stretching is, and

the initial field geometry, but for any large-scale field rearrangement the fraction will be significant, so we suggest $0.1 < \beta \lesssim 1$. Note that $\beta > 1$ is also quite possible: it means the Meissner-expelled state is of lower energy than the pre-condensation field $\boldsymbol{B}_0$. Recall that reconnection will not occur for a pre-condensation field less than $\sim 10^{12}$ G. In addition, the requisite field-line stretching needed to produce sharp features on which reconnection can act will not occur if the pre-condensation field $\gtrsim H_c$. The value of B_0 cannot be converted to a precise pre-condensation magnetic energy because this depends on the quantitative field structure, but we can approximate it as some average magnetic energy density $\bar{B}_0^2/8\pi$ multiplied by the volume of the star,

$$\mathcal{E}^0_{\rm mag} \approx \frac{\bar{B}_0^2 R_*^3}{6} = 2.9 \times 10^{41} \left(\frac{\bar{B}_0}{10^{12}\,{\rm G}}\right)^2 \left(\frac{R_*}{12\,{\rm km}}\right)^3 {\rm erg}. \tag{43}$$

Summarizing the arguments of this subsection, the kind of reconnection event required to produce a Meissner-expelled magnetic field will release somewhere in the range

$$\mathcal{E}_{\rm mag} \approx \alpha\beta \times \left(2.9 \times 10^{41} - 7.2 \times 10^{46}\right) {\rm erg} \tag{44}$$

of energy, where the parameters α and β are most likely to be of order unity. In the following section, we will make quantitative calculations of the former. The above energy release will coincide with the onset of superconductivity, i.e. after a few minutes. Although the supernova is still very bright at this stage, this rather specific signature could potentially be detectable – or at least constrained. Furthermore, exactly when it occurs would provide a valuable constraint on the variety of different energy gap models, as it would lead directly to an estimate of the maximum value of T_c (Lander et al. 2024). Although enhanced cooling is also a signature of the start of Cooper pairing, and neutron–neutron pairing may be responsible for the current thermal evolution of the Cas A NS (whose age is around 350 yr, Page et al. 2011; Ho et al. 2015), the corresponding effect due to proton–proton pairing would occur so close to birth as to be masked by the still-bright supernova. The possible energy injection discussed here is therefore the only plausible possibility for observationally constraining the proton gap model.

4 A QUANTITATIVE MODEL FOR FIELD REARRANGEMENT

Any of the above scenarios could, potentially, be realized, with the details depending on the pre-condensation magnetic field, the internal fluid motion of the star, and the efficiency of reconnection mechanisms. We now consider a simple concrete example where all calculations are semi-analytic, to get some quantitative results.

The most general axisymmetric poloidal magnetic field satisfying the solenoidal constraint $\nabla \cdot \boldsymbol{B} = 0$ takes the form

$$\boldsymbol{B} = \nabla u \times \boldsymbol{e}_\phi, \tag{45}$$

where $u = u(r, \theta)$ is the poloidal stream function. Note that from equation (45),

$$\boldsymbol{B} \cdot \nabla u = 0, \tag{46}$$

which implies that $u =$ const along a given field line. Every field line can therefore be labelled the value $u = u_0$ along it, which will be convenient later. This value lies in the range $0 \le u \le u_{\rm max}$, where $u = 0$ for $\theta = 0$ and $u_{\rm max}$ is attained at the centre of the equatorial region of closed field lines, at which the poloidal magnetic-field strength drops to zero.

In the case of a dipolar magnetic field in magnetohydrostatic equilibrium in an $N = 1$ polytropic star, Monaghan (1965) found

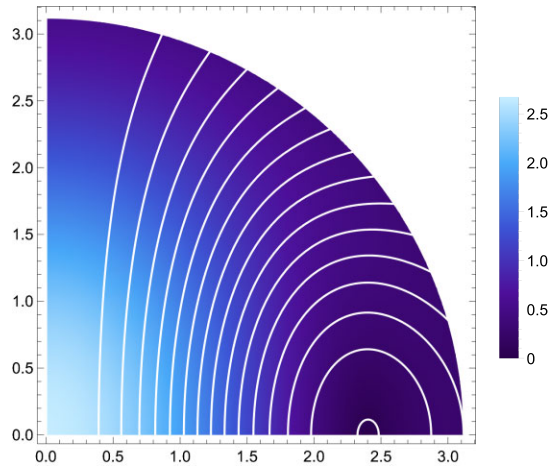

Figure 4. A purely poloidal field in hydromagnetic equilibrium in an $N = 1$ polytropic star. The surface of the star is at a radius $r = \pi$, in the usual dimensionless units used in the Lane–Emden equation. Colour scale shows the magnitude of the field; and white lines show contours of constant value of the stream function, equivalently, the magnetic-field lines.

the following analytic solution for the stream function:

$$u = \mathfrak{B} \sin^2\theta \left(\frac{4\sin\xi}{\xi} - 4\cos\xi - 2\xi\sin\xi - \frac{2\xi^2}{3}\right), \tag{47}$$

where $\mathfrak{B}$ is an arbitrary constant setting the magnitude of the magnetic field and ξ is the usual dimensionless radius from the solution to the Lane–Emden equation (2). We plot the magnitude and direction of the resulting magnetic field in Fig. 4. Note that the inclusion of more realistic equations of state and thermal pressure contributions result in only minor deviations from this simple model (Lander et al. 2021).

To evaluate the magnetic energy along a flux tube (equation 19), we need a way to parametrize position along a given field line. We cannot use the stream function u, because a field line is defined by $u =$ const. Each field line is a set of 2D coordinates $\{r, \theta\}$, so if we can express either of the coordinates as a function of the other, i.e. $r = r(\theta)$ or $\theta = \theta(r)$, this will give us a satisfactory parametrization to use.

Looking at Fig. 4 and imagining drawing spokes radially outwards from the origin (i.e. lines of $\theta =$ const), we see that in general (it is easiest to visualize in the equatorial region of closed field lines), a single spoke passes through the same field line in two places, so writing $r = r(\theta)$ would map one radial value to two positions on the field line, and therefore $r(\theta)$ violates the definition of a function and we cannot use θ for location along a given field line $u = u_0$. Instead imagining concentric circles of constant r, we see that each of these crosses a single field line in just one location; reversing the previous logic means that we can parametrize position along any given field line $u =$ const $\equiv u_0$ by r. We may now evaluate the magnetic energy along a flux tube (equation 19), but it is informative to start with the simpler calculation of the length of a field line, stretched and unstretched. We present the details for the case of advecting field lines towards the equator, as in Fig. 2; the case of stretching field lines towards the pole is a trivial modification to the calculation (and we will give results for this case too).

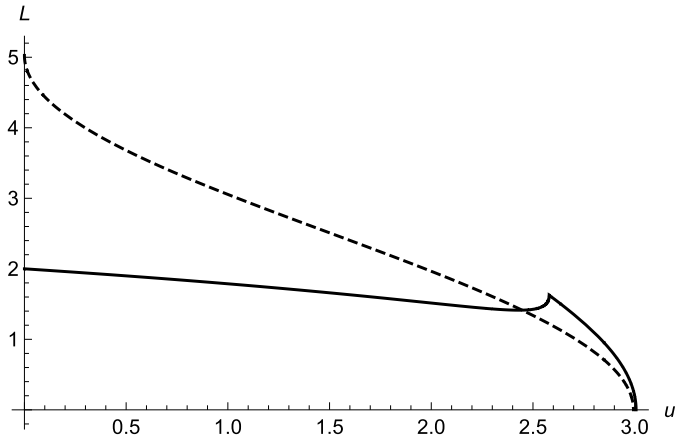

Figure 5. Length of unstretched field lines L_1 (solid line) and the additional stretched component L_2 (dashed line), in dimensionless units divided by π, as a function of the constant value of the stream function labelling each field line, from the straight field line running from pole to pole ($u_0 = 0$), past the start of the closed-field-line region $u_0 \approx 2.6$ to the maximum value at the centre of the closed-field-line region $u_0 \approx 3.0$.

Using a standard result for lengths of parametrized curves, an unstretched field line $u = u_0$ has length

$$L_1(u_0) = 2 \int_{r_{\rm min}}^{r_{\rm max}} \sqrt{1 + r^2 \left(\frac{{\rm d}\theta(r, u_0)}{{\rm d}r} \right)^2}\, {\rm d}r, \tag{48}$$

where the integration is carried out only in the quadrant shown in Fig. 4, exploiting the equatorial symmetry of the field, so the factor of 2 gives the full length of the field line. The length of the additional stretched component is simply twice that of the circular arc from where the field line intersects the radius $r = \mathcal{R}$ to the equator $\theta = \pi/2$, i.e.

$$L_2(u_0) = 2\mathcal{R} \left(\frac{\pi}{2} - \theta(\mathcal{R}, u_0) \right). \tag{49}$$

We plot L_1 and L_2 for field lines throughout the star in Fig. 5. To understand this plot, recall that every field line can be labelled the value $u = u_0$ along it. The field line with $u = 0$ is the straight line along the magnetic-field symmetry axis, which runs from pole to pole. Moving away from this axis u increases,[4] reaching the value $u_0 = (2\pi^2 - 12)/3$ at which field lines begin to close inside the star. Moving further into the closed-field-line region u continues to increase, and reaches a maximum $u = u_{\rm max} \approx 3.0069$ at the centre of the closed-field-line region. In the dimensionless units used, the radius of the star is at a value π. We therefore expect the straight field line running from pole to pole to have a length equal to the diameter of the star, 2π, and for the length to drop to zero at the centre of the closed-field-line region; this is seen in Fig. 5 for the unstretched field line L_1. There is not a monotonic decrease in field-line length from $u = 0$ to $u_{\rm max}$: a small cusp is seen corresponding to the transition from open to closed field lines (only the length inside the star is measured, otherwise it would be a smooth decrease at the transition). If the field lines are maximally stretched towards the equator and back at the radius of onset of superconductivity fixed at $\mathcal{R} = 0.8R_*$, as shown in Fig. 2, the additional length is the value L_2 plotted. The field line running along the symmetry axis should have its length increased by $0.8\pi \times 2\pi \approx 5.0\pi$, which agrees with the plot, and this stretched component decreases to zero for field lines progressively closer to the equator (which therefore have less distance to cover), as expected.

Stretching magnetic-field lines increases the energy of the configuration; recall Section 3.4. It is informative to think of this process through the contributions of individual field lines, or more specifically a thin volume with length given by the magnetic-field line and some infinitesimal cross-sectional area ${\rm d}A$. We will refer to the integral of the magnetic energy density $B^2/8\pi$ along a field line multiplied by ${\rm d}A$ as the 'magnetic energy of the field line' and denote this $\mathfrak{E}_{\rm mag}$. For the Monaghan field, combining the contributions from the unstretched piece $\mathfrak{E}^0_{\rm mag}$ and the stretched region $\mathfrak{E}^{\rm str}_{\rm mag}$ for a given field line $u = u_0$ gives us:

$$\begin{aligned} \mathfrak{E}_{\rm mag} = \mathfrak{E}^0_{\rm mag} + \mathfrak{E}^{\rm str}_{\rm mag} = \Bigg\{ & 2 \int_{r_{\rm min}}^{r_{\rm max}} \left[\frac{B(r, \theta(r))]^2}{8\pi} \sqrt{1 + r^2 \left(\frac{{\rm d}\theta(r, u_0)}{{\rm d}r} \right)^2}\, {\rm d}r \right. \\ & + \left. 4\mathcal{R} \left(\frac{\pi}{2} - \theta(\mathcal{R}, u_0) \frac{[B(\mathcal{R}, \theta(\mathcal{R}, u_0))]^2}{8\pi} \right) \right\} \times {\rm d}A, \end{aligned} \tag{50}$$

where we have combined equations (21), (48), and (49). In the calculations that follow, we set the pre-factor $\mathfrak{B}$ from equation (47) to unity. This results in no loss of generality, as we are interested in the fractional increase in magnetic energy per field line for a given starting magnetic field, so the $\mathfrak{B}$ factors cancel from numerator and denominator in such a ratio. There is also no qualitative difference between the field-line structure at different field strengths.

Fig. 6 shows that the increase in $\mathfrak{E}_{\rm mag}$ is not simply proportional to the increased length of the field line, because the field strength at the point where the superconducting shell begins varies across the star. For $\mathcal{R}$ further in, the total increase in field-line length is reduced, but because the field strength is higher towards the centre, the magnetic energy per field line is actually increased. We notice that the energy increases are far greater if field lines are stretched towards the equator rather than the pole. This is because in the former case, the field lines that are most stretched are those in regions of strong magnetic field; and in the latter case, the most stretching is from the closed-field-line region, where B is small (and drops to zero in the centre).

This calculation is in dimensionless units, but because the magnetic-field structure is the same at any field strength, the results can be readily rescaled. The key result will be quantifying the fractional increase in total magnetic energy α in the two cases

[4]Actually, as defined in the Monaghan solution, u drops from zero along the axis to being negative definite everywhere else. When referring to specific values of the stream function we actually quote the absolute value $|u|$ to avoid confusion when referring to the 'maximum' value $u_{\rm max}$.

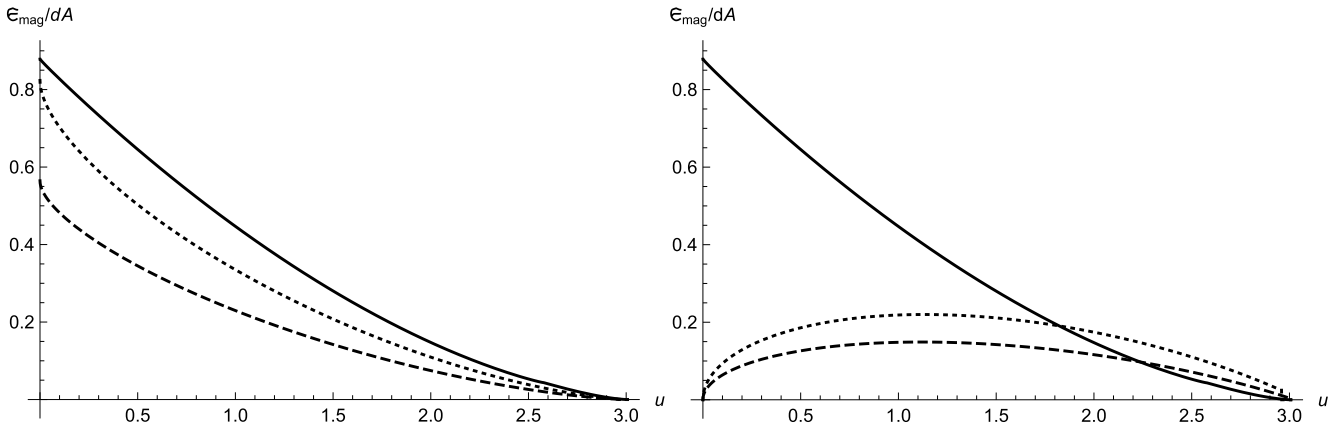

Figure 6. Energy per field line as a function of value $u = u_0$. Unstretched field shown with the solid line, dashed (dotted) lines show the additional magnetic energy for each field line due to the stretched piece of the field when $\mathcal{R} = 0.8\pi$ (0.7π). Left-hand panel shows the increase in energy by stretching field lines towards $\theta = \pi/2$; and right-hand panel shows the corresponding energy increases resulting from stretching field lines towards $\theta = 0$.

where the field is stretched in the onset shell of superconductivity. Note, however, this quantitative calculation adds nothing new to our understanding of the efficacy of reconnection, i.e. the β parameter from equation (44) describing the amount of magnetic energy that is ultimately released.

We now want to understand the total increase in magnetic energy when all the field lines across the shell $r = \mathcal{R}$ are suitably distorted towards either the equator or pole. Similarly to the calculation for the length of a field line (equation 48), we may also calculate the area of the surface of revolution obtained from rotating this field line through an angle of 2π radians in the azimuthal direction:

$$S_1(u_0) = 2\int_{r_{\rm min}}^{r_{\rm max}} 2\pi x(r)\sqrt{1 + r^2\left(\frac{{\rm d}\theta(r,u_0)}{{\rm d}r}\right)^2}\,{\rm d}r$$
$$= 4\pi\int_{r_{\rm min}}^{r_{\rm max}} r\sin\theta(r)\sqrt{1 + r^2\left(\frac{{\rm d}\theta(r,u_0)}{{\rm d}r}\right)^2}\,{\rm d}r. \quad (51)$$

Finally, the whole volume of the star can then be described as a set of nested surfaces of revolution, each with constant u and with an infinitesimal spacing du between them – that is, the volume of the star V is given by the integral

$$V = \int_{u=0}^{u_{\rm max}} S_1(u)\,{\rm d}u. \quad (52)$$

Similarly, we will find the magnetic energy of the original magnetic field $\mathcal{E}^0_{\rm mag}$ and the additional stretched component $\mathcal{E}^{\rm str}_{\rm mag}$ by first evaluating the following functions (note that these differ from the $\mathfrak{E}_{\rm mag}$ functions in their extra $2\pi r\sin\theta(r)$ surface area element in the integrand) for a given field line $u = u_0$:

$$E_0(u_0) = \frac{1}{2}\int_{r_{\rm min}}^{r_{\rm max}} B^2 r\sin\theta(r)\sqrt{1 + r^2\left(\frac{{\rm d}\theta(r,u_0)}{{\rm d}r}\right)^2}\,{\rm d}r, \quad (53)$$

$$E_{\rm str}(u_0) = 8\pi\mathcal{R}^2\sin\theta(\mathcal{R},u_0)\left(\frac{\pi}{2} - \theta(\mathcal{R},u_0)\frac{[B(\mathcal{R},\theta(\mathcal{R},u_0))]^2}{8\pi}\right), \quad (54)$$

and then integrating these over u:

$$\mathcal{E}^0_{\rm mag} = \int_{u=0}^{u_{\rm max}} E_0(u)\,{\rm d}u, \quad (56)$$

$$\mathcal{E}^{\rm str}_{\rm mag} = \int_{u=0}^{u_{\rm max}} E_{\rm str}(u)\,{\rm d}u, \quad (57)$$

In practice, we find consistent inaccuracies with this approach. The volume calculated from equation (52) is 4.8 per cent greater than the exact value of $4\pi^4/3$ for a sphere of radius $R_* = \pi$, and the magnetic energy for the pre-condensation field calculated in the same manner, from equation (56), is 29 per cent greater than the straightforward volume integral[5] of the energy density:

$$\frac{1}{8\pi}\int_{\phi=0}^{2\pi}\int_{\theta=0}^{\pi}\int_{r=0}^{R_*} B^2 r^2\sin\theta\,{\rm d}r{\rm d}\theta{\rm d}\phi. \quad (59)$$

These discrepancies seem to stem from a shortcoming of parametrizing a field line as $r = r(\theta)$, since although this is formally a satisfactory choice (as discussed earlier), towards the equator field lines become tangential to contours of constant radius – so a substantial change in field-line location becomes a very small change in radius. To check whether the parametrization was at fault or an error in our calculations, we tried a different magnetic-field configuration with straight vertical lines, and in this case, the integral of field-line contributions over the range of values of the stream function did yield the correct results for volume and magnetic energy. This gives us confidence that the method of calculation is not itself at fault and, although the resulting 29 per cent inaccuracy in the energy is undesirable, it is likely to affect the calculations of both $\mathcal{E}^0_{\rm mag}$ and $\mathcal{E}^{\rm str}_{\rm mag}$ in a similar manner. Since we are interested in the fractional increase in magnetic energy, $\alpha = \mathcal{E}^{\rm str}_{\rm mag}/\mathcal{E}^0_{\rm mag}$, the systematic inaccuracies in both numerator and denominator are likely to cancel each other out to a large extent, resulting in a ratio that is reliable to our order of working. In Table 1 we present values for α for a range of plausible values of the radius $\mathcal{R}$ of the nascent superconducting shell.

Returning to the arguments of Section 3.8, any reconnection event will be accompanied by the release of a substantial amount of energy. To quantify this, we now need to convert from dimensionless to cgs

[5]In fact the magnetic energy evaluated both in this conventional way and via the field-line parametrization should both take the radial integration out to infinity; but the result of stopping at the surface should be the same for both methods.

units. Using the fact that the dimensionless radius $\hat{r}$ and magnetic field at the polar cap $\hat{B}_{\rm p}$ are given by

$$\hat{r} = \frac{\pi r}{R_*}\,,\ \hat{B}_{\rm p} = \frac{B_{\rm p}}{\mathfrak{B}} = \frac{4}{3} - \frac{8}{\pi^2}, \tag{60}$$

we simply need to multiply these quantities by a pre-factor to yield the physical ones:

$$r = 3.2 \times 10^5 \hat{r} R_{12}\ {\rm cm}\,,\ B_{\rm p} = 1.9 \times 10^{12} \hat{B}_{\rm p} B_{12}\ {\rm G}. \tag{61}$$

Two other useful relations are obtained from the dimensionless magnetic energy $\hat{\mathcal{E}}^0_{\rm mag} = 5.4937$. We can use it to define an average internal magnetic field $\hat{\bar{B}}$, and hence find the ratio of polar cap to average internal field, which is the same in both dimensionless and physical units:

$$\frac{\bar{B}}{B_{\rm p}} = \frac{\hat{\bar{B}}}{\hat{B}_{\rm p}} = \frac{1}{\hat{B}_{\rm p}}\sqrt{\frac{8\hat{\pi}\hat{\mathcal{E}}^0_{\rm mag}}{V}} = 1.972. \tag{62}$$

We can also calculate magnetic energy from equation (56) in physical units, which entails multiplying by $B_{\rm p}^2 R_*^3$, giving us:

$$\mathcal{E}^0_{\rm mag} = 6.5 \times 10^{41} \left(\frac{B^0_{\rm p}}{10^{12}\,{\rm G}}\right)^2 \left(\frac{R_*}{12\,{\rm km}}\right)^3\ {\rm erg}. \tag{63}$$

For simplicity, let us assume that all the additional energy from field-line stretching is released, i.e. $\beta = 1$. In the case of the stretch towards the equator, full reconnection is possible, and depending on where the initial shell of superconductivity $\mathcal{R}$ is located (which in turn depends upon the gap model), the value of α will differ (see Table 1). This leads to a predicted energy release in the range

$$\mathcal{E}^{\rm out}_{\rm 1i} = (3.5 - 6.0) \times 10^{43}\ B^2_{\rm p,13}\ {\rm erg}. \tag{64}$$

For our fiducial model with $\mathcal{R} = 0.79$, the pre-factor in the above expression is 4.8. In the case of stretching towards the pole, however, we do not expect substantial reconnection – let us take $\beta = 0.1$ for the sake of definiteness – and Table 1 shows us that α is also a little smaller in this case, and so we estimate

$$\mathcal{E}^{\rm out}_{2} = (0.33 - 0.51) \times 10^{43}\ B^2_{\rm p,13}\ {\rm erg} \tag{65}$$

in this latter case, with a pre-factor of 0.39 for the fiducial model. However such an energy release manifests itself, it will clearly produce a rather weaker signal. Finally, scenarios 1ii and 3 both assume reconnection is at best feeble, and so in these cases negligible energy release would be expected at the onset of superconductivity.

Earlier on we used the requirement of flux conservation together with $B \leq H_c$ to calculate the angular extent of any $B \neq 0$ hole through the otherwise Meissner-expelled superconducting shell, culminating in equations (40) and (41). This general treatment of flux conservation can now also be made specific to the Monaghan field, whose flux through a spherical shell of given radius is plotted in Fig. 7; note that the maximum value of the magnetic flux occurs at a radius very close to that of the onset of superconductivity for our fiducial model. For the post-rearrangement phase we made the assumption that $B^2_\perp = B^2_\parallel$, but one can see visually that for the specific model considered here, the field is virtually radial at a radius of 0.79π (and near to the equator, where the angular component is relatively large, the overall magnitude is close to zero). We quantify the typical value of $B^2_\parallel / B^2_\perp$ with the ratio

$$\frac{\int_0^{\pi/2} B^2_\parallel(\mathcal{R},\theta)\,{\rm d}\theta}{\int_0^{\pi/2} B^2_\perp(\mathcal{R},\theta)\,{\rm d}\theta} = 0.0048 \text{ for } \mathcal{R} = 0.79\pi. \tag{66}$$

The criterion for overcoming superconductivity, written in terms of $B_\perp$, then becomes

$$B_\perp = \frac{H_c}{\sqrt{1.0048}} = H_c \text{ to our order of accuracy.} \tag{67}$$

Otherwise we follow the same working as before, which for scenario 2 leads to a polar hole opening angle of

$$\theta_{\rm open} = \arccos\left(1 - \frac{\mathfrak{F}_0}{4\pi\mathcal{R}^2 H_c}\right) \tag{68}$$

and for scenario 1ii, an equatorial ring of half-angular thickness

$$\theta_{\rm eq} = \arccos\left(\frac{\mathfrak{F}_0}{4\pi\mathcal{R}^2 H_c}\right). \tag{69}$$

Both these angles are plotted in Fig. 8 as a function of field strength, for the Monaghan field and our fiducial model for superconductivity.

Were the field strength in the inner and outer regions to remain constant as the superconducting region expands, then by flux conservation through the polar hole (or equatorial ring), the $B \neq 0$ zone within the superconducting shell would be of constant cross-sectional area, i.e. a cylindrical hole in the case of scenario 2. However, because the expansion of the superconducting shell also decreases the volume of the inner and outer normal regions, flux conservation also implies that the field will be 'concentrated' and amplified. We explore this next.

5 LATER EVOLUTION

5.1 Field evolution in NS cores

The expansion of the superconducting shell, in every case except scenario 3, drives an amplification of the magnetic field in the $B \neq 0$ regions, as described in the following subsection. The time-scale for this process depends on the specific superconducting gap profile, but at least the early phase should proceed over a mere few years after birth, considerably faster than any other mechanism for core-field evolution. At later times, if the critical temperature drops significantly towards the centre of the star, the Meissner-induced field amplification may slow down considerably, and it becomes important to understand whether this process might work in tandem with other field-evolution processes in the core.

Core field evolution is a contentious topic, with a variety of approaches that lead to wildly different estimates for the characteristic evolutionary time-scale: as short as 10^3 yr (e.g. Castillo, Reisenegger & Valdivia 2020) and at least as long as 10^{11} yr (e.g. Graber et al. 2015). This is not our primary focus here, but a review of recent literature suggests that the only short-time-scale mechanisms assume normal matter (i.e. non-superconducting protons and non-superfluid neutrons, Castillo et al. 2020; Moraga et al. 2024). Earlier work suggesting short-time-scale evolution in a superconducting core (e.g. Jones 2006) has recently been criticized, with counter-arguments suggesting far slower evolution (Passamonti et al. 2017; Gusakov 2019), at least if the star is static (Gusakov, Kantor & Ofengeim 2020).

We conclude that the dynamic Meissner effect considered in this paper will, in general, not add to this discordance, as it should be completed well before even the fastest plausible core-field evolution mechanisms have begun their work. In particular, for the specific approximate critical temperature profile we adopt, the transition to superconductivity is completed (in the regions where it can be completed) in a matter of a few decades.

Table 1. Fractional increase in magnetic energy, $\mathcal{E}^{\rm str}_{\rm mag}/\mathcal{E}^{0}_{\rm mag}$, as a function of position of superconducting shell $\mathcal{R}$. We consider a plausible range of values of $\mathcal{R}$ in increments of $0.05R_*$, and also the 'fiducial' model with $\mathcal{R} = 0.79R_*$. In the dimensionless units used in the calculation, the pre-condensation magnetic energy $\mathcal{E}^{0}_{\rm mag} = 5.4937$.

Position of $\mathcal{R}$	0.9	0.85	0.8	0.79	0.75	0.7
$\mathcal{E}_{\rm mag}$ increase from field lines stretched towards equator	0.5380	0.6267	0.7212	0.7411	0.8233	0.9271
$\mathcal{E}_{\rm mag}$ increase from field lines stretched towards pole	0.5029	0.5436	0.5930	0.6058	0.6704	0.7817

5.2 Compression of flux

Whichever of our four scenarios for field rearrangement (recall Fig. 3) is realized, the later evolution will be dictated by this initial shell formation. If flux penetrates the shell, it will continue to do so as the shell expands, a process which we will assume, for simplicity, does not change the field structure itself within that region (a related issue is touched upon in Section 6.1). In all cases except scenario 3, the volume of the star threaded by the macroscopic field decreases as the superconducting shell expands. In ideal MHD, however, Alfvén's frozen-flux theorem dictates that expulsion of magnetic flux would have to be accompanied by expulsion of the fluid too! Instead, Alfvén's theorem can only be valid for the normal proton fluid, which is strongly coupled to the (non-superfluid) neutron fluid too. Over a transition region into the superconducting shell, where $T \lesssim T_c$, but $T \ll T_c$, the proton fluid will behave like an admixture of normal and superconducting components, as for the two-fluid model of liquid helium; fluid elements will effectively start to be able to slip across field lines rather than being permanently threaded by them. This phase deserves further study; for now, we simply point out that without this re-definition of Alfvén's theorem, there can be no development of the Meissner effect in the thickening superconducting shell.

With this revised Alfvén's theorem, the expansion of the superconducting shell pushes field lines beyond the outer boundary $r = R_{\rm out}$ further outwards, and inner field lines $r < R_{\rm in}$ further inwards. We can see by flux conservation that this will necessarily amplify the magnetic field. More precisely, since the expansion of the superconducting shell is radial, we will also assume the magnetic field is pushed radially inwards/outwards. We cannot apply Eulerian flux conservation, i.e. across a shell of fixed radius, because the region hosting the flux is shrinking from its initial radial extent of $\mathcal{R}$ for the inner sphere ($R_* - \mathcal{R}$ for the outer shell). Instead we need to consider Lagrangian flux conservation. Let R_1 be the radius of some arbitrary spherical shell at the onset of superconductivity, $R_{\rm in}$ and $R_{\rm out}$ the inner and outer radii of the superconducting shell some time later, and $\mathcal{R}$ the radius of the initial shell of superconducting matter. Then Lagrangian flux conservation means that the magnetic flux through the shell $r = R_1$ at the onset of superconductivity should be equal to the flux through a different shell $r = R_2$ once the superconducting shell has expanded, where

$$R_2 = \begin{cases} \frac{R_{\rm in}}{\mathcal{R}} R_1 & \text{for } R_1 < \mathcal{R}, \\ R_* - \frac{(R_* - R_{\rm out})}{(R_* - \mathcal{R})}(R_* - R_1) & \text{for } R_1 > \mathcal{R}. \end{cases} \tag{70}$$

Flux conservation is then expressed as

$$\mathfrak{F}_1 \equiv R_1^2 \int B_r(R_1, \theta, \phi)\, {\rm d}\theta {\rm d}\phi = R_2^2 \int B_r(R_2, \theta, \phi)\, {\rm d}\theta {\rm d}\phi \equiv \mathfrak{F}_2$$

$$\Rightarrow \frac{\int B_r(R_2, \theta, \phi)\, {\rm d}\theta {\rm d}\phi}{\int B_r(R_1, \theta, \phi)\, {\rm d}\theta {\rm d}\phi} = \left(\frac{R_1}{R_2}\right)^2 \quad \text{for } R_1 < \mathcal{R}, \tag{71}$$

$$\frac{\int B_r(R_* - R_2, \theta, \phi)\, {\rm d}\theta {\rm d}\phi}{\int B_r(R_* - R_1, \theta, \phi)\, {\rm d}\theta {\rm d}\phi} = \left(\frac{R_* - R_1}{R_* - R_2}\right)^2 \quad \text{for } R_1 > \mathcal{R}. \tag{72}$$

In the special case where the radial magnetic field is a separable function, of the form $B(r, \theta, \phi) = f(r)g(\theta)h(\phi)$ – which includes the Monaghan field – the above expressions reduce to considerably simpler forms:

$$\frac{B_r(R_2)}{B_r(R_1)} = \left(\frac{R_1}{R_2}\right)^2 \text{ for } R_1 < \mathcal{R}\,, \quad \frac{B_r(R_* - R_2)}{B_r(R_* - R_1)} = \left(\frac{R_* - R_1}{R_* - R_2}\right)^2 \text{ for } R_1 > \mathcal{R}. \tag{73}$$

Note that we have to be careful to choose a shell within one of the normal-matter regions, because along the boundary shells at $r = R_{\rm in}$, $r = R_{\rm out}$ the flux is zero, so flux conservation here does not give any information about the amplification of B due to the expansion of the superconducting shell. Finally, although we have found a relation for the amplification of B_r, if we assume the field geometry is unchanged by this compression, then the other components of $\boldsymbol{B}$ must also be magnified in the same way. On the other hand, even if the other field components are assumed not to be amplified in the same way, they must still be excluded from the superconducting shell – ingredients for the possible (and perhaps inevitable) development of current sheets; we will therefore dismiss this possibility, and so regard the previous relation as applying to the magnitude of the total magnetic field and not just its radial component. We can then combine equations (70) and (73) to give

$$B(R_2) = \left(\frac{\mathcal{R}}{R_{\rm in}}\right)^2 B(R_1) \text{ for } R_1 < \mathcal{R}\,, \quad B(R_* - R_2) = \left(\frac{R_* - \mathcal{R}}{R_* - R_{\rm out}}\right)^2 B(R_* - R_1) \text{ for } R_1 > \mathcal{R}\,. \tag{74}$$

5.3 Final state after flux compression

The flux compression described above cannot continue indefinitely, as it will eventually result in a magnetic field with $B = H_c$. At this point, the expansion of the superconducting shell is arrested, and the final configuration from scenarios 1i, 1ii, and 2 is dictated by this. Along the way to reaching this final state, as the magnetic field is amplified, this also affects the opening angle of the polar holes/equatorial ring from scenarios 1ii and 2. We discuss whether these regions are actually normal or superconducting in the following subsection.

Let us solve to find this post-compression state for the Monaghan field. This field does not have a spatially constant magnitude B, nor does any self-consistent equilibrium solution, making it less obvious which quantity should be equated with H_c to determine when compression must cease. Here, we will simply assume this occurs when

$$\bar{B} \equiv \sqrt{\frac{1}{V_{\rm inner}} \int_{V_{\rm inner}} B^2\, {\rm d}V} = H_c. \tag{75}$$

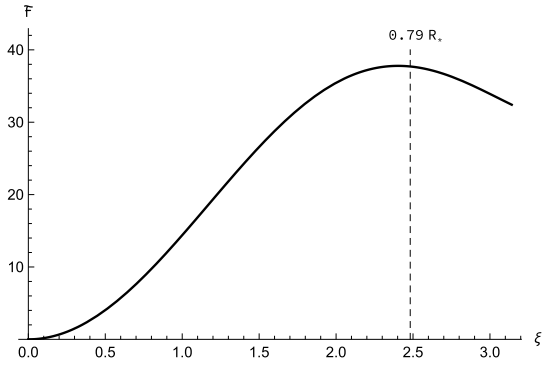

Figure 7. Magnetic flux through a spherical surface of constant radius, as a function of dimensionless radius ξ in the star. The onset of superconductivity in our fiducial model is marked.

We combine this with equation (74) to find the final radius of the $B \neq 0$ inner region:

$$R_{\rm in} = \mathcal{R}\sqrt{\frac{\bar{B}_1}{H_c}}, \tag{76}$$

where $\bar{B}_1$ is the average field strength of the inner region $r < \mathcal{R}$ at the onset of superconductivity. A similar calculation can be done for the outer normal region, but in this case the radius is not necessarily constrained by flux conservation, since the outer $0.1R_*$ of the radius of the star will be normal in any case. So the inner radius of the outer normal region is

$$R_{\rm out} = \min\left\{0.9R_*,\, R_* - (R_* - \mathcal{R})\sqrt{\frac{\bar{B}_1}{H_c}}\right\}. \tag{77}$$

As well as this inner core, we note that the crustal field is also somewhat increased by the flux being pushed outwards, by a factor of 4.4 for the Monaghan field and our fiducial model for superconductivity; only in the case of $B_p = 10^{14}$ G does this outer region exceed the critical field and lead to the outer boundary $R_{\rm out}$ of the superconducting region being a little in from the crust–core boundary, as seen in the right-hand panel of Fig. 10. The variation of $R_{\rm in}$ and $R_{\rm out}$ with average internal field strength is plotted in Fig. 9. This completes the description of the final state for scenario 1i.

For another of the four scenarios, scenario 3, there is no calculation to perform: we assume flux threads the entire star on a macroscopic scale, and so flux conservation does not impose any restrictions on the final state of the magnetic field. This leaves scenarios 1ii and 2. In both these cases, $R_{\rm in}$ and $R_{\rm out}$ are the same as for scenario 1i, but we also need to calculate the spatial extent of the polar holes/equatorial ring. Because the angles $\theta_{\rm open}, \theta_{\rm eq}$ depend on the magnetic field, which in turn is amplified by flux compression, we cannot just use a calculation based on the radius of the nascent superconducting shell $\mathcal{R}$; the angular extent of these $B \neq 0$ regions will change as the shell expands. In practice, these can be calculated by replacing $\mathcal{R}$ in equations (68) and (69) with the changing $R_{\rm in}$ and $R_{\rm out}$, to build up a full 2D meridional cut through the star of the $B = 0$ region at the end of the flux-compression phase. This region is shown shaded in purple in Fig. 10 for three different field strengths within the range where Meissner expulsion is possible, with polar-cap values $B_{\rm p} = 10^{12}$, 10^{13}, and 10^{14} G, for the case of $B \neq 0$ polar holes, and so completes the description of the end state for scenario 2. The change in opening angle throughout the shell is subtle but noticeable (the boundaries of the holes are visibly slightly curved). Scenario 1ii, the equatorial ring, is identical in the 2D plot except that the plots need to be rotated by an angle of $\pi/2$.

5.4 Are $B \neq 0$ core regions normal or superconducting?

Throughout this paper, we have avoided discussing the state of the core region inside the $B = 0$ superconducting shell (for scenarios 1i, 1ii, and 2), and the $B \neq 0$ regions within that shell (for scenarios 1ii and 2) – specifically, whether these $B \neq 0$ parts of the stellar core are in a normal or superconducting state. This issue is less important within the narrow focus of the current work, and by side-stepping it, we avoid a potentially involved discussion about the differences between flux structures in type-I and type-II superconductors, and normal matter. The same issue also affects the nature of the core in scenario 3. The intention is to confront this issue alongside the general $B \sim H_c$ case, in a follow-up paper. Here, we simply assume flux compression results in a final state where $B = H_c$ in these regions.

The state of these $B \neq 0$ core regions is, however, potentially crucial for related issues, such as the interactions with the superfluid neutrons in these regions (Lander et al. 2024), so warrants at least some brief speculation. The state is likely determined by evolutionary processes, and understanding it is probably inhibited by our simplistic assumption that $H_c = $ const and that we can perform calculations using an average value for the magnetic field $\bar{B}$.

More realistically, the inner region $r < R_{\rm in}$ starts normal with a field strength that is likely to peak near/at the centre of the star and decrease away from it. Flux compression will halt further encroachment of the superconducting shell into this region once the outer part has reached – probably – a lower critical field, H_{c1} and H_{c1} (type-I and II, respectively). The outer part of the $r < R_{\rm in}$ core would then be superconducting, but instead of having $B = 0$ would be in the intermediate state, where flux penetrates through small-scale flux structures. In the very central region, however, flux compression may have taken B above the upper critical field by that point – in which case the matter will remain normal (it does not 'break' superconductivity, as it never entered that state).

If flux compression has this effect, then it would imply that the $B \neq 0$ holes in the superconducting shell would also be superconducting and in the intermediate state where flux penetration is possible – i.e. the entire shell is superconducting, but with just one or two contiguous regions threaded by field lines.

6 TOROIDAL COMPONENT AND HIGHER MULTIPOLES

6.1 Toroidal and linked poloidal–toroidal fields

We have argued that the key early phases of field rearrangement depend on the magnetic-field component that crosses the nascent shell of superconductivity. As long as the star is approximately spherical, $B_\perp \approx B_r$. A toroidal field is, by definition, perpendicular to the radial direction – so would not evolve through any scenario involving fluid motion, making its later evolution simpler. Either it would simply be enveloped by the expanding superconducting shell, i.e. scenario 3 in our terminology, or could be 'cut' across the incipient superconducting shell without any need for rearrangement through advection (since toroidal field lines are tangential to spherical shells, including the incipient superconducting shell). In this latter case, however, matching the field to zero across a boundary would require a surface current whose magnitude would scale with the field strength.

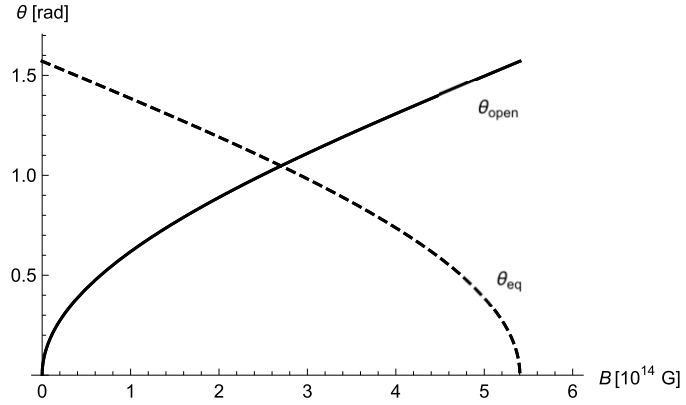

Figure 8. Opening angles for $B \neq 0$ regions within the superconducting shell, in scenarios 1ii ($\theta_{\rm eq}$, the dashed line) and 2 ($\theta_{\rm open}$, the solid line), as a function of field strength. $\theta_{\rm open}$ increases with field strength until it reaches the equator. $\theta_{\rm eq}$ begins at the equator, $\theta = \pi/2$, so for increasing field strength its value decreases, as it expands out towards the symmetry axis running from pole to pole.

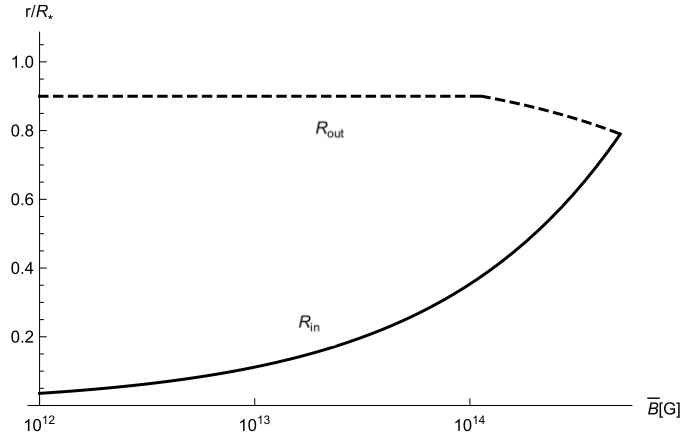

Figure 9. Inner and outer radii of the final superconducting shell, as a function of field strength.

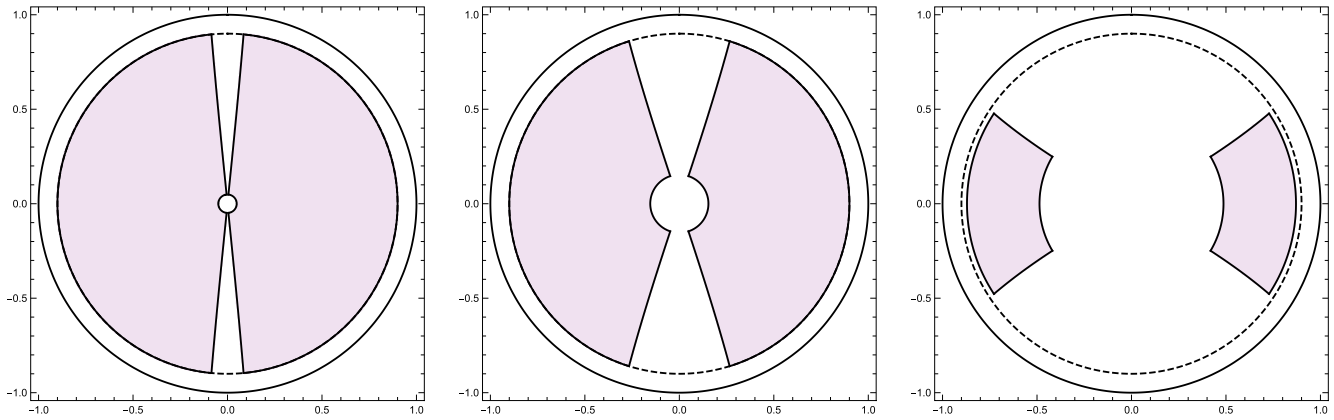

Figure 10. The final structure of the superconducting region, after flux compression has finished, for scenario 2 (shaded purple region). Scenario 1ii has an identical structure in this 2D plane, but rotated through $\pi/2$, so that the Northern and Southern polar 'holes' in the Meissner shell then become a single equatorial ring where the Meissner effect is not present; scenario 1i only has the central region with magnetic field and no breaks in the shell. For this end state, the average field strength of the inner region will be $H_c = 5 \times 10^{14}$ G. Note that whilst the crust (outside the dashed circle but within the solid circle) is always composed of normal matter, the white core regions could either be normal matter or superconducting matter threaded by field lines (the minimum-energy state for stronger fields than those we consider).

Its later evolution, including field amplification in the inner core and crustal regions, would follow that of scenario 1i, as discussed in Section 5 and plotted in Fig. 9. There is no reason for scenarios 1ii and 2 to be realized, i.e. if there is a Meissner-expelled region, it is likely to be a complete shell, without $B \neq 0$ holes. The effect of the expanding superconducting shell on a purely toroidal field, in scenario 1i, is sketched in Fig. 11.

Which field configuration is most likely? Purely poloidal and purely toroidal magnetic fields are both unrealistic, both because there is no plausible formation scenario for these, and also because they are unstable on dynamical time-scales (Wright 1973; Tayler 1973), so we now consider linked poloidal–toroidal fields where the poloidal component is at least 'significant' (not necessarily dominant).

The requirement $\nabla \cdot \boldsymbol{B} = 0$ already reduces $\boldsymbol{B}$ to having two degrees of freedom, poloidal and toroidal, and axisymmetry further reduces this to one. In particular, the poloidal stream function u becomes the single variable, and the toroidal field is expressed as a function of u. This means that the toroidal component takes a constant value along any contour of u, i.e. a poloidal field line. The total extent of the region with a toroidal component is usually chosen to be demarcated by the largest field line that closes within the star, to avoid having the current distribution extending outside the star (Lander & Jones 2009). As seen earlier (recall Fig. 3), the superconducting transition results in various possible scenarios for the rearrangement of poloidal field lines. In the closed-field-line region, when a toroidal component is added, these closed loops in the plane of the page become spiral-shaped field lines that extend into the azimuthal direction, and any fluid flow driving the rearrangement will advect these complete field lines, not just their poloidal or toroidal components (the latter case would also require surface currents to allow for abrupt jumps across the normal-superconducting boundaries). Therefore, the toroidal component must adjust to the rearranging closed poloidal field lines: one can imagine simply 'filling in' this region with toroidal field. Doing so, we see that for scenario 1i we will be left with two disconnected regions of toroidal field, on the inside and outside of the superconducting shell. In scenario 1ii, these regions will be joined across the equatorial $B \neq 0$ belt to leave a region with a dumbbell-shaped cross-section where the toroidal field resides. In both scenarios 2 and 3, the details of the closed-field-line rearrangement depend on the exact pre-condensation field geometry and the location of the incipient shell of superconductivity, but we believe the mostly likely result is a small region of toroidal field confined to the crust alone. All these possibilities are sketched in Fig. 12. Note the similarity of scenario 3, where poloidal fields are all open in the core and the toroidal field is confined to the crust, to earlier equilibrium models for a magnetic-field threading the entire stellar interior and $B < H_c$ (Lander 2014).

This more realistic geometry deserves more attention, however, as the toroidal component is not simply passive during the rearrangement, but will play at least two roles itself. One is that the stronger the toroidal component, the more it acts to shrink its host closed poloidal-field region (Lander & Jones 2009; Armaza, Reisenegger & Valdivia 2015) – thus, a very strong pre-condensation toroidal component is more likely to be confined to a radius $r > \mathcal{R}$, which – following the onset of superconductivity – will be pushed outwards, so that the only toroidal field remaining at the end of the Meissner phase is in the crust. The other role the toroidal field will play is through its contribution to the overall B^2, thus exceeding the critical field more easily in the closed-field-line region and invalidating our earlier approximation that $B \approx$ const along $r = \mathcal{R}$.

6.2 Higher multipole pre-condensation magnetic fields

If the magnetic field is dominated by higher multipoles, unlike the dipolar configuration we have assumed, the characteristic length-scale of the field will become correspondingly shorter, affecting the likely final state of the magnetic field. Let us assume for definiteness a spherical harmonic expansion of the field, with the largest amplitude contribution being some particular harmonic Y_l^m. The characteristic angular scale $\mathcal{L}_\parallel$ for the field will be reduced from $\mathcal{L}_\parallel \sim \pi$ for the dipole field to $\mathcal{L}_\parallel \sim \pi/l$ for the (l, m) harmonic (recall that $|m| \leq l$, so it is π/l and not π/m that gives the minimum angular scale).

For the higher multipole field, the distance one must stretch a field line until it encounters an oppositely directed neighbouring field line is reduced from $\sim \pi/2$ (recall the cartoon of Fig. 3) to $\sim \pi/(2l)$. Progressively less fluid motion is, therefore, required to achieve this as the multipolar index increases; in this sense it becomes 'easier' to realize scenario 1i for full Meissner expulsion. The efficacy of reconnection is, however, unaffected, since it depends upon the thickness of the reconnection zone (i.e. its radial extent, in this context) $\mathcal{L}_\perp$ rather than $\mathcal{L}_\parallel$.

Scenarios 1ii and 2 will have a more complex structure for a higher multipole field; instead of being pierced once or twice, as for the dipole field, we anticipate that the number of normal 'holes' in the superconducting shell will scale with l and m. The higher the multipolar index, the more likely it is that the star will end up in scenario 3 (which can be thought of as the limiting case of scenario 1ii or 2 in the limit of very large l, m).

7 DISCUSSION AND OUTLOOK

One might find the Meissner-effect scenario proposed here implausible, relying as it does on an interplay of two pieces of physics – field-line advection and reconnection – whose modelling is difficult and only outlined here. But the motivation for this paper was not a frivolous survey of contrived scenarios for this phase, but rather to ask the question: is there any way to produce a Meissner-expelled region on a short time-scale? If the answer had been no, we would have had to conclude that essentially all numerical work on magnetic-field evolution in the crust – a field of research built up over the last two decades (e.g. Hollerbach & Rüdiger 2002; Pons & Geppert 2007; Perna & Pons 2011; Ascenzi et al. 2024) – would have been suspect, and magnetar modelling would potentially need substantial revision (without rapid crustal evolution, one would need to return to earlier ideas of core evolution involvement, but the latter process is likely to be even slower). On the other hand, had our conclusion been that the dynamical-time-scale Meissner expulsion explored here is always effective, theoretical modelling of NS rotation would have faced challenges (Lander et al. 2024). The model proposed here allows for both extremes, as well as intermediate scenarios where a Meissner-expelled shell is broken by one or two regions through which field penetrates.

Even if more detailed future work were to show the Meissner mechanism proposed here to be ineffective, much of our discussion about the necessary conditions for macroscopic field expulsion would remain relevant. For example, Ohmic decay alone reduces magnetic energy but does not obviously have any way to induce the kind of field rearrangement needed to produce a zero-field region. If, therefore, one wishes to invoke Ohmic decay as a mechanism for flux transport and Meissner expulsion (as in earlier studies), one must still confront some of the same issues discussed in this paper. In particular, the solenoidal constraint on the magnetic field will

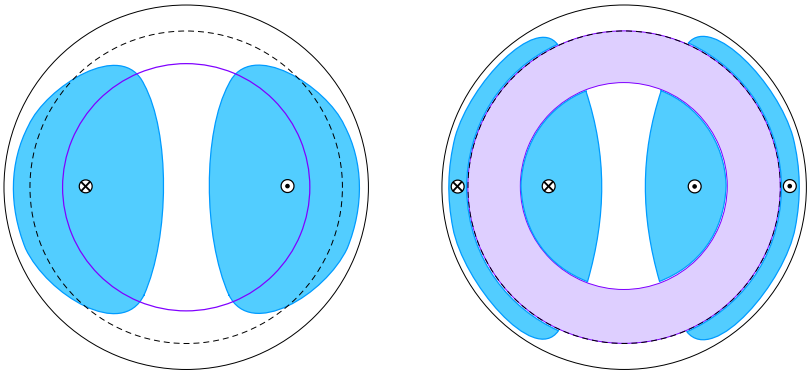

Figure 11. A purely toroidal field has field lines everywhere perpendicular to poloidal lines, and so orthogonal to the page in this meridional plot, and is non-zero within some region like the two blue lobes plotted here. At the onset of superconductivity (left), the toroidal field on either side of the incipient superconducting shell can be matched to zero by having a surface current at both inner and outer boundaries; cf. Fig. 3. As the shell expands (right), a complete Meissner-expelled shell can be formed without any additional dynamics other than compression of flux in the crust, and in the inner core region.

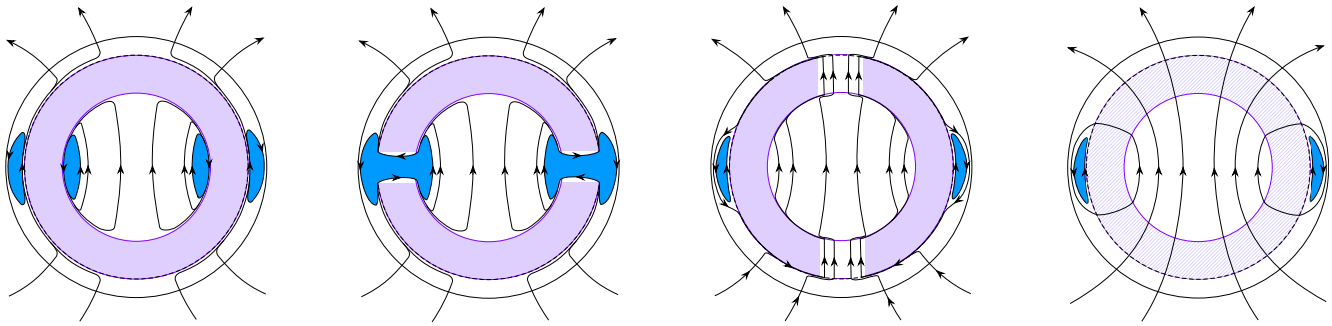

Figure 12. Sketch of the location of the toroidal component (plotted as blue lobes) of a linked poloidal-toroidal field in each of the purely-poloidal-field scenarios shown in Fig. 3. Left to right: scenarios 1i, 1ii, 2, and 3.

again restrict how the field can be expelled, as will (on appropriate time-scales/length-scales) flux conservation.

Previous work on the Meissner effect has focused on local dynamics, whether a small region is uniformly penetrated by flux (the normal state), irregularly penetrated (by thin flux tubes whose dimensions are universal, in the case of type-II superconductivity; or other flux structures, in the case of type-I superconductivity), or fully expelled (Ho et al. 2017). The problem is particularly rich when the proton superconductor co-exists with a neutron superfluid (Haber & Schmitt 2017; Wood & Graber 2022), as expected after a few hundred years (beyond the phase of primary interest to us here). But we argue here that additional restrictions need to be considered on the macroscopic scale, related to the field geometry, and only then can one predict whether a given flux-transport mechanism could produce a field-expelled region. These also lead to restrictions on the minimum field strength for which we expect Meissner expulsion: both the field-line advection phase and the reconnection phase require the same value, $B \gtrsim 10^{12}$ G. This means that although, in principle, one might expect partial Meissner expulsion for lower field strengths than full expulsion (in the case of ineffective reconnection, scenarios 1ii and 2), in practice this is not realized. However, we emphasize that $B \gtrsim 10^{12}$ G does not imply the star will host a Meissner-expelled region, only that it is possible. A closer examination of the likelihood of each of the two stages in our Meissner model (advection and reconnection) will help to assess how plausible each of the scenarios is, in practice. In contrast with the lower limit on B, the upper limit is not given by macroscopic arguments, but rather is the same as that for local calculations, the critical field strength. However, our macroscopic calculations for a Meissner-expelled region with a $B \neq 0$ hole do also naturally reach the limit of no expelled field in the case of $B \approx H_c$. Once the field strength reaches H_c – or if it is already globally this strong before the onset of superconductivity – the problem becomes more subtle. There is no longer a single clear minimum-energy state of $B = 0$, and the resulting configuration will be an interplay between whatever the new minimum-energy state is – be it flux tubes, lamellae, or other flux structures – and the advection and reconnection physics needed to realize this state. A realistic model of the NS core would, in fact, likely involve an inner core region of type-I superconductivity, a type-II superconducting outer core, a normal crust, and suitable conditions to describe the interface between each of these. We intend to return to this $B \sim H_c$ case in a future study.

There are reassuring similarities between our scenario 3 and previous work on $B < H_c$ equilibrium magnetic-field configurations in a type-II superconductor (Roberts 1981; Henriksson & Wasserman 2013; Lander 2014), showing that in this limit of our modelling, the field naturally leads to the development of a global hydromagnetic equilibrium. In cases with partial or complete Meissner expulsion, the expected configurations are qualitatively different. Scenario 1i features a disconnected inner region of poloidal and toroidal field, and in scenario 1ii, a $B \neq 0$ equatorial band through the field-expelled shell potentially allows for penetration of the toroidal component into the core even in the case of relatively weak B; a core toroidal component was previously found not to occur below $\sim 10^{14}$ G (Lander 2013, 2014). For scenario 2, on the other hand, even in the case $B > 10^{14}$ G, the toroidal component is likely to

be confined to the crust. Finally, we showed that a stronger pre-condensation toroidal field is more likely to be confined to the crust post-condensation.

The model presented here invokes an unmodelled fluid flow to rearrange magnetic-field lines prior to reconnection, and the nature of this fluid flow deserves detailed scrutiny in the future. Some residual dynamics from birth are to be expected, but whether this is the leading mechanism driving field-line advection remains to be seen. What is clear is that the axisymmetric model considered here is likely to be overly simplistic, since a near-incompressible flow $\nabla \cdot \boldsymbol{v} \approx 0$ moving consistently towards (say) the equator in one meridional plane would have to travel some distance in the azimuthal direction and then circulate away again. This simplistic flow, together with the assumed initially dipolar field, make the realization of Meissner state in the sketches here seem rather contrived and unlikely. However, this is just a limiting case that is conceptually simpler. In reality, the more multipolar and small-scale the pre-condensation field and fluid flow are, the easier it will be to produce partial or complete Meissner expulsion. None the less, some features of the simple model, including the restriction on the range of internal field strengths and the need for an inner $B \neq 0$ core of matter underneath the Meissner shell, are expected to be robust.

Some of the ideas explored here have crossover with similar notions from stellar dynamos. In both cases, one is concerned with understanding how a suitable MHD flow can be rearranged and reconnected into a new configuration, and a detailed treatment inevitably involves assumptions about the nature of the small-scale field to be reconnected (Rincon 2019). Both the dynamo and the Meissner-expulsion phase of an NS are further complicated by the high magnetic Prandtl number of the flow (Lander 2021). Another interesting, related problem from fluid dynamics that may have relevance to understanding the advection phase of our Meissner model is that of the expulsion of magnetic flux by an eddy (Weiss 1966; Galloway & Weiss 1981).

This paper focuses on development of the theory of a dynamical Meissner effect. A companion letter (Lander et al. 2024), explores some of the interesting observational consequences of this model.

ACKNOWLEDGEMENTS

I thank Danai Antonopoulou, Vanessa Graber, Kostas Gourgouliatos, and Zorawar Wadiasingh for helpful discussions on some aspects of this work.

DATA AVAILABILITY

The data underlying this article will be made available upon reasonable request.

REFERENCES

Annett J. F., 2004, Superconductivity, Superfluids and Condensates. Oxford Univ. Press, Oxford
Armaza C., Reisenegger A., Valdivia J. A., 2015, ApJ, 802, 121
Ascenzi S., Viganò D., Dehman C., Pons J. A., Rea N., Perna R., 2024, MNRAS, 533, 201
Baym G., Pethick C., Pines D., 1969a, Nature, 224, 673
Baym G., Pethick C., Pines D., 1969b, Nature, 224, 674
Burrows A., Lattimer J. M., 1986, ApJ, 307, 178
Castillo F., Reisenegger A., Valdivia J. A., 2020, MNRAS, 498, 3000
Chamel N., 2008, MNRAS, 388, 737
Chen J. M. C., Clark J. W., Davé R. D., Khodel V. V., 1993, Nucl. Phys. A, 555, 59
Cutler C., Lindblom L., 1987, ApJ, 314, 234
Douchin F., Haensel P., 2001, A&A, 380, 151
Flowers E., Itoh N., 1979, ApJ, 230, 847
Galloway D. J., Weiss N. O., 1981, ApJ, 243, 945
Glampedakis K., Andersson N., Samuelsson L., 2011, MNRAS, 410, 805
Glampedakis K., Andersson N., Lander S. K., 2012, MNRAS, 420, 1263
Graber V., Andersson N., Glampedakis K., Lander S. K., 2015, MNRAS, 453, 671
Gusakov M. E., 2019, MNRAS, 485, 4936
Gusakov M. E., Kantor E. M., Ofengeim D. D., 2020, MNRAS, 499, 4561
Haber A., Schmitt A., 2017, Phys. Rev. D, 95, 116016
Henriksson K. T., Wasserman I., 2013, MNRAS, 431, 2986
Hirsch J. E., 2012, Phys. Scr., 85, 035704
Ho W. C. G., Glampedakis K., Andersson N., 2012, MNRAS, 422, 2632
Ho W. C. G., Elshamouty K. G., Heinke C. O., Potekhin A. Y., 2015, Phys. Rev. C, 91, 015806
Ho W. C. G., Andersson N., Graber V., 2017, Phys. Rev. C, 96, 065801
Hollerbach R., Rüdiger G., 2002, MNRAS, 337, 216
Jafari A., Vishniac E. T., Kowal G., Lazarian A., 2018, ApJ, 860, 52
Jones P. B., 2006, MNRAS, 365, 339
Kowal G., Lazarian A., Vishniac E. T., Otmianowska-Mazur K., 2009, ApJ, 700, 63
Lander S. K., 2013, Phys. Rev. Lett., 110, 071101
Lander S. K., 2014, MNRAS, 437, 424
Lander S. K., 2021, MNRAS, 507, L36
Lander S. K., Jones D. I., 2009, MNRAS, 395, 2162
Lander S. K., Haensel P., Haskell B., Zdunik J. L., Fortin M., 2021, MNRAS, 503, 875
Lander S. K., Gourgouliatos K. N., Wadiasingh Z., Antonopoulou D., 2024, preprint (arxiv:2411.08020)
Lazarian A., Vishniac E. T., 1999, ApJ, 517, 700
Mendell G., 1991, ApJ, 380, 515
Mestel L., 2012, Stellar Magnetism. Oxford Univ. Press, Oxford
Monaghan J. J., 1965, MNRAS, 131, 105
Moraga N. A., Castillo F., Reisenegger A., Valdivia J. A., Gusakov M. E., 2024, MNRAS, 527, 9431
Page D., Geppert U., Weber F., 2006, Nucl. Phys. A, 777, 497
Page D., Prakash M., Lattimer J. M., Steiner A. W., 2011, Phys. Rev. Lett., 106, 081101
Parker E. N., 1957, J. Geophys. Res., 62, 509
Passamonti A., Akgün T., Pons J. A., Miralles J. A., 2017, MNRAS, 469, 4979
Perna R., Pons J. A., 2011, ApJ, 727, L51
Pons J. A., Geppert U., 2007, A&A, 470, 303
Rincon F., 2019, J. Plasma Phys., 85, 205850401
Roberts P. H., 1981, Q. J. Mech. Appl. Math., 34, 327
Sedrakian A., Clark J. W., 2019, Eur. Phys. J. A, 55, 167
Sweet P. A., 1958, in Lehnert B., ed., Vol. 6, Electromagnetic Phenomena in Cosmical Physics, p. 123
Tayler R. J., 1973, MNRAS, 161, 365
Tilley D., Tilley J., 2019, Superfluidity and Superconductivity. Routledge
Tinkham M., 2004, Introduction to Superconductivity. Courier Corporation
Weiss N. O., 1966, Proc. R. Soc. Lond. Ser. A, 293, 310
Wood T. S., Graber V., 2022, Universe, 8, 228
Wright G. A. E., 1973, MNRAS, 162, 339

This paper has been typeset from a TEX/LATEX file prepared by the author.